• U C •

FCTUC FACULDADE DE CIÊNCIAS
E TECNOLOGIA
UNIVERSIDADE DE COIMBRA

DEPARTAMENTO DE
ENGENHARIA MECÂNICA

Design of the Valve Actuation Mechanism of a Four-Stroke Spark Ignition Internal Combustion Engine

Submitted in Partial Fulfillment of the Requirements for the Degree of Master in Mechanical Engineering in the specialty of Energy and Environment

Selecção e Dimensionamento de um Mecanismo de Accionamento de Válvulas de um Motor de Combustão Interna de Ciclo de 4 Tempos de Ignição por Faísca

Author

Francisco José Queirós Capela de Vieira e Brito

Advisor

Professor Doutor Pedro de Figueiredo Vieira Carvalheira

Jury

President	**Professor Doutor José Manuel Baranda Moreira da Silva Ribeiro** **Professor Auxiliar da Universidade de Coimbra**
Vowels	**Professor Doutor Fernando Jorge Ventura Antunes** **Professor Auxiliar da Universidade de Coimbra** **Professor Doutor Pedro de Figueiredo Vieira Carvalheira** **Professor Auxiliar da Universidade de Coimbra**
Advisor	**Professor Doutor Pedro de Figueiredo Vieira Carvalheira** **Professor Auxiliar da Universidade de Coimbra**

Coimbra, July, 2016

With your mind power, your determination, your instinct, and the experience as well, you can fly very high.

Ayrton Senna, in “Racing is in My Blood”, 1991.

To my Parents and Joana.

ACKNOWLEDGEMENTS

This dissertation would not be possible without all the support I received. I would like to take this opportunity and repay some of that gratitude.

To my Advisor, Professor Doutor Pedro Carvalheira. For the incredible support, availability and concern from the first moment, but also for teaching me so much in such a short span of time. I could not have hoped for a better advisor. Thank you very much Professor.

To my Parents. Not only for supporting me all of the time and allowing me to pursue my dreams, but also for being a daily inspiration and a true example that belief and hard work can accomplish anything. Thank you so much.

To Joana. For being everything I could ask for and more. For the incredible support in every second I need it and for encouraging me to be better every single day. Thank you so much.

Abstract

The goal of this work is to design the valve actuation mechanism of a naturally aspirated, four-stroke, spark ignition internal combustion engine, for an urban vehicle. The engine has a 1.0-liter displacement volume, three cylinders inline, with four valves per cylinder and port fuel injection.

The work began by performing numerical simulations using software developed at DEM-FCTUC [1]. This software models the engine cycle to determine the valve lift and valve opening and closing angles. The simulations are performed in the engine torque and speed domain of use, for the functional requirements of the engine. Two architectures of the valve actuation mechanism were defined. The kinematic and dynamic studies were then made, and the friction power of the two mechanisms, as a function of engine speed, was evaluated. Afterwards the architecture was selected. The following components of the actuation mechanism were object of detailed design in Autodesk Inventor 2016: intake and exhaust valves, intake and exhaust valve springs, bucket tappets, valve retainers, valve keepers, valve beads, valve guides and valve seats.

Keywords Engine, Valve, Variable, Lift, Intake, Exhaust, Bucket Tappet, Finger Follower, Mechanism.

Resumo

A motivação para este trabalho consiste em efetuar a seleção e o projeto detalhado de um mecanismo de acionamento de válvulas de um motor de combustão interna, de ciclo de quatro tempos e ignição por faísca, para um veículo automóvel utilitário. O motor tem 1.0 litro de cilindrada, três cilindros em linha, quatro válvulas por cilindro e injeção na porta de admissão.

O trabalhou começou pela realização de simulações de modelação do ciclo de funcionamento do motor, usando o programa "Ciclo de Funcionamento do Motor" desenvolvido no DEM-FCTUC [1], para determinar o levantamento máximo e os ângulos de abertura e fecho das válvulas de admissão e escape em função da velocidade de rotação do motor. Foram definidas duas arquiteturas para o trem de válvulas, efetuados estudos cinemáticos e dinâmicos e avaliado o atrito de ambos os mecanismos em função da velocidade de rotação do motor. De seguida foi efetuada a seleção da arquitetura mais adequada, em função dos requisitos funcionais do mesmo. Os componentes seguintes do mecanismo de acionamento das válvulas do motor foram objeto de desenho pormenorizado em software de desenho CAD-3D (Autodesk Inventor 2016): válvulas de admissão e de escape, molas das válvulas de admissão e escape, touches, retentores das válvulas, pratos das válvulas, meias-luas, guias das válvulas e sedes das válvulas.

Palavras-chave: Motor, Válvula, Variável, Levantamento, Admissão, Escape, Touche, Balanceiro, Mecanismo.

Contents

LIST OF FIGURES

LIST OF TABLES

SIMBOLOGY AND ACRONYMS

Simbology

A – Ultimate strength of the spring wire for a wire diameter of 1 mm

a – Bucket tappet's top thickness

β – Valve seat angle

D – Average spring diameter

d – Spring wire diameter

D_{ie} – Exhaust valve inner seat diameter

D_{ii} – Intake valve inner seat diameter

D_s – Valve stem diameter

D_{se} – Exhaust valve stem diameter

D_{si} – Intake valve stem diameter

D_{ve} – Exhaust valve external seat diameter

D_{vi} – Intake valve external seat diameter

DE_{BT} – Bucket tappet outer diameter

DI_{BTG} – Bucket tappet guide inner diameter

DI_{VG} – Valve guide inner diameter

E – Modulus of elasticity

F_{cam} – Cam force

F_{damping} – Damping force

F_{pe} – Pressure force on the exhaust valves

F_{pi} – Pressure force on the intake valves

F_{pressure} – Pressure force

F_{seat} – Valve seat force

F_{spring} – Spring force

$F(t)$ – Resulting force

F_{weight} – Weight force

G – Torsional modulus of elasticity

g – Gravitational acceleration

K_d – Damping coefficient

K_{dBT} – Bucket tappet damping coefficient

K_{dVG} – Valve guide damping coefficient

K_s – Spring rate

L – Valve spring length for a given x

$L_{(x=0)}$ – Valve spring length when $x = 0$/Maximum length of the valve spring after being assembled between the upper and lower valve plates

L_0 – Free length of the valve spring

L_{BT} – Bucket tappet length

L_{VG} – Valve guide length

m – Total mass of the system

$m_{\mathrm{bead\ locks}}$ – Mass of the bead locks

$m_{\mathrm{bucket\ tappet}}$ – Mass of the bucket tappet

m_{spring} – Mass of the valve spring

m_{spring} – Spring mass

m_{sw} – Exponent of the wire diameter for ultimate strength of spring wire

$m_{\mathrm{upper\ plate}}$ – Mass of the upper plate

$m_{\mathrm{upper\ plate}}$ – Upper plate mass

m_{valve} – Mass of the valve

m_{valve} – Valve mass

N_a – Number of active coils

n – Engine speed

n_{cyl} – Number of cylinders

n_f – Fatigue safety factor

p_{atm} – Atmospheric pressure

P_b – Brake Power

p_c – Pressure inside the cylinder

p_e – Pressure on the outlet port

p_i – Pressure on the inlet port

r_c – Compression ratio

S_a – Alternate strength

S_e – Endurance strength

S_m – Average strength

S_{sa} – Alternate shear strength

S_{se} – Endurance shear strength

S_{sm} – Average shear strength

S_{su} – Ultimate shear strength

S_{ut} – Ultimate strength

T – Temperature

T_b – Brake torque

V_{cc} – Volume of the combustion chamber

V_d – Engine displacement volume

V_{dc} – Cylinder displacement volume

x – Valve lift/displacement

x_0 – Difference in length between L_0 and $L_{(x=0)}$

w – Valve seat width

σ_a – Alternate stress

σ_m – Average stress

τ_a – Alternate shear stress

τ_m – Average shear stress

$\tau_{1\mathrm{max}}$ – Maximum value of shear stress amplitude

$\tau_{1\mathrm{min}}$ – Minimum value of shear stress amplitude

τ_1 – Shear stress amplitude

ν – Poisson's ratio

$\mu(T)$ – Dynamic viscosity of oil

Acronyms

ABDC – After Bottom Dead Center

ATDC – After Top Dead Center

BBDC – Before Bottom Dead Center

BDC – Bottom Dead Center

bsfc – Brake Specific Fuel Consumption

BTDC – Before Top Dead Center

BTV – Butterfly Throttle Valve

CAD – Computer Aided Design

DEM – Departamento de Engenharia Mecânica

DOHC – Dual/Double Overhead Camshaft

ECU – Engine Control Unit

EVC – Exhaust Valves Close

EVL – Exhaust Valve Lift

EVO – Exhaust Valves Open

FCTUC – Faculdade de Ciências e Tecnologia da Universidade de Coimbra

ICE – Internal Combustion Engine

IVC – Inlet Valves Close

IVL – Intake Valve Lift

IVO – Inlet Valves Open

RPM – Revolutions Per Minute

SI – Spark Ignition

SOHC – Single Overhead Camshaft

TDC – Top Dead Center

TI – Ignition Timing

UMM – União Metalo-Mecânica

VTEC – Variable Valve Timing and Lift Electronic Control

VVEL – Variable Valve Event and Lift

VVL – Variable Valve Lift

VVT-i – Variable Valve Timing with Intelligence

WOT – Wide Open Throttle

1. INTRODUCTION

1.1. Motivation

Nowadays, there is a total absence of internal combustion engine projects in Portugal. The desire to build genuine Portuguese engines and motor vehicles has always been on the minds of several engineers and automotive enthusiasts. Portuguese engine and car manufacturing - despite some interesting and notable examples – Alba (Figure 1.1), Casal, UMM, etc. - has always fallen short of its true potential. An incomprehensible reality when the large number of countries that target this type of industry are analyzed.

The automotive industry is one of the most important in the world and it offers a wide range of solutions for almost every costumer need. Urban vehicles are one of the most popular ones. Not only do they influence the daily lives of innumerous families, but they also play an important role on the impact that motor vehicles have in the environment.

Figure 1.1. Alba, a Portuguese manufactured car between 1952 and 1954, racing at the Caramulo hill climb in 2007 [2].

Environmental problems such as global warming, are a worrying reality and a worldwide concern. Among many other aspects in a car, the engine is one of critical relevance to the environmental issue. It is therefore utmost important to design an internal combustion engine with the lowest possible fuel consumption and emission levels. The rules regulating vehicle emissions are tight and tend to become even more in the future. For 2020, the European Union's CO_2 emissions target is 95 grams per kilometer (for passenger cars) [3]. To comply with these regulations (Figure 1.1), engine manufacturers are investing on a number of solutions which allow them to boost the efficiency of their engines. One of those solutions is engine downsizing, which is a growing worldwide trend in urban vehicles. More and more manufacturers are including small engines in their powertrain catalogue, showing this is the way to go. Their goal is simple: build a small and highly efficient power unit.

Although these are very important issues, it is also necessary for the car to be as attractive as possible for the driver. For that to happen, the engine must produce a decent amount of brake power. One of the most popular technologies to achieve the desired brake power throughout the engine's operating range is cam phasing. To further increase brake power, but also to lower both fuel consumption and emission levels, variable valve lift is applied to the valve train. Variable valve lift allows the engine to lower its brake specific fuel consumption in partial load.

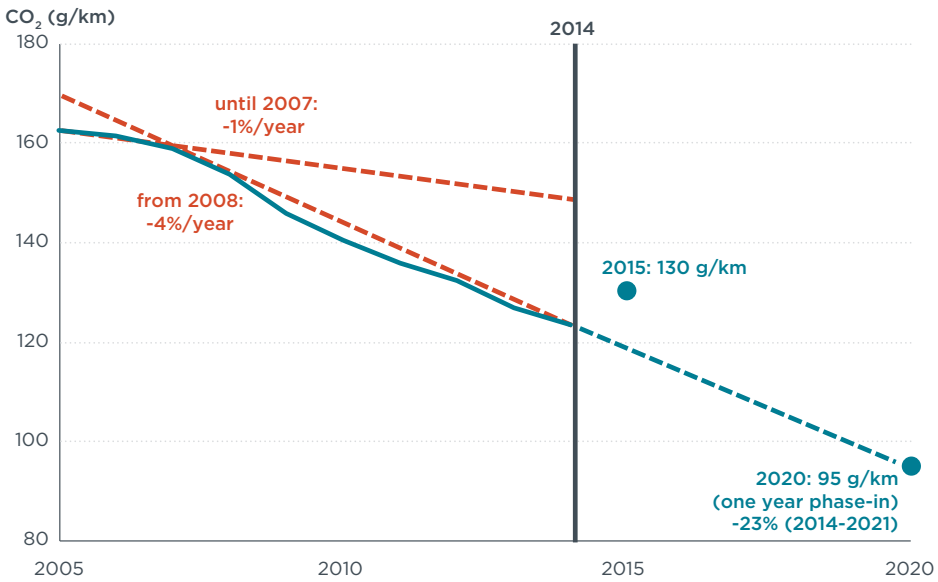

Figure 1.2. EU's CO2 emissions goal for 2020 [4].

1.2. Goals

The present dissertation aims to suppress the absence of national projects in the automotive industry, by providing the first insight on what will be a complete and detailed project of an internal combustion engine for an urban vehicle. This work focuses on the analysis, selection and design of the engine's valve train.

1.3. Starting Point

When it comes to urban vehicles, there are many different types of motoring options adopted by manufacturers. A preliminary study carried out in [5] focused on comparing the different types of solutions available, and was able to determine which SI (spark ignition) engine best fits an urban vehicle. It concluded that the best engine would be an inline three-cylinder with a displacement volume around 1.0-liter. As a future work proposal it was suggested that the engine's detailed project and CAD (computer aided design) were made. These conclusions and future work proposals are the starting point of this dissertation.

1.4. Methodology

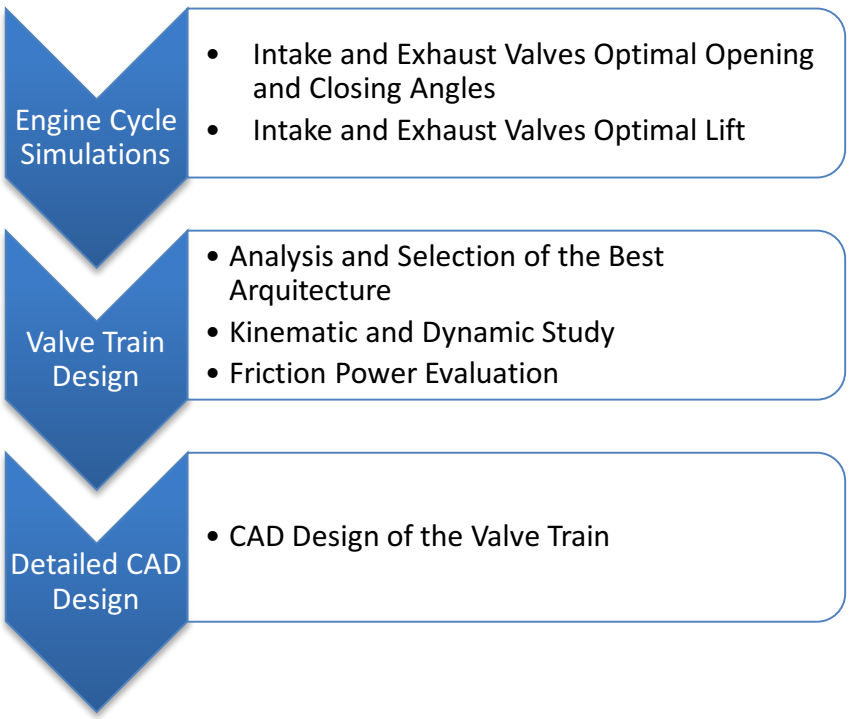

Figure 1.3. Work methodology.

The first step of the work methodology (Figure 1.3) is to model the engine cycle in order to obtain the optimal opening and closing angles (for the intake and exhaust valves) and the optimal values of valve lift in the engine torque and speed domain of use, for the engine's functional requirements. The work is followed by the analysis of two different types of architectures for the valve actuation mechanism. A kinematic and dynamic study is performed for both valve train architectures, as well as a friction power evaluation of both mechanisms as a function of engine speed (n). After the best architecture is selected, the work is concluded with the design of the valve train mechanism.

1.5. Definition of Engine Characteristics

Some of the engine's characteristics have already been defined in [5]. To this point, those characteristics are:

- Four-Stroke;
- Spark Ignition;
- Inline three-cylinder;
- A displacement around 1.0-liter;

However, before the valve train can be addressed, there are several other characteristics that need to be addressed and justified. To do this, the specifications of several engines (that meet the above list of characteristics) are analyzed. The analyzed engines are:

Table 1.1. Analyzed engines characteristics: displacement; stroke; bore; stroke/bore; air induction.

	Displacement [cm^3]	Stroke [mm]	Bore [mm]	Stroke/Bore	Air Induction
Ford EcoBoost	999	82.0	71.9	1.140	Turbocharged
Opel Ecotec Turbo	999	77.4	74.0	1.046	Turbocharged
Volkswagen TSI	999	76.4	74.5	1.025	Turbocharged
Nissan DIG-S	1198	83.6	78.0	1.072	Supercharged
PSA (group) PureTech	1199	90.5	75.0	1.206	Turbocharged
Renault Energy TCe 90	898	73.1	72.2	1.012	Turbocharged
Honda ECA Series 3-cyl.	995	81.5	72.0	1.132	Atmospheric
Toyota 1KR-FE	998	84.0	71.0	1.183	Atmospheric
Smart Fortwo	999	81.8	72.0	1.136	Atmospheric

Air Induction

It is concluded from (Table 1.1), that the majority of inline three-cylinder SI engines have forced induction air intake (whether its turbocharged or supercharged) making it a rational solution due to its popularity among car manufacturers. However, this is not the only important factor when deciding what type of air intake the engine will have. As previously stated in this work's goals, this project aims to suppress a lack of nationally designed engines. Nowadays, Portuguese industry has no tradition whatsoever in building internal combustion engines and it is important to offer a simpler solution before trying to build a more complex one. Like many car manufacturers, before a turbocharged/supercharged engine is designed, a naturally aspirated/atmospheric engine must be build. Therefore, an atmospheric engine is chosen.

Bore and Stroke

The analysis of both bore and stroke is based on the L/B ratio.

$$\frac{L}{B} > 1 \tag{1.1}$$

Being:

L – Stroke

B – Bore

If the stroke/bore ratio's value is closer to 1 (as is the case with both the Renault Energy TCe 90 and the Opel Ecotec Turbo), the specific power increases but the efficiency decreases. If that is not the case, the efficiency is higher, while the specific power is lower. Having already decided upon a naturally aspirated engine, and giving priority to the engine's efficiency, **the chosen ratio is 1.183**, as in the 1KR-FE engine. Of all atmospheric engines that were analyzed, the 1KR-FE is the one with the highest L/B ratio (and therefore, with the highest efficiency). The **bore** and **stroke** values are **71.0 mm** and **84.0 mm**, respectively.

Table 1.2. Analyzed engines characteristics: valve train; valves per cylinder; compression ratio; fuel injection.

	Valve Train	Valves per Cylinder	Compression Ratio	Fuel Injection
Ford EcoBoost	DOHC	4	10.0:1	Direct Fuel Injection
Opel Ecotec Turbo	DOHC	4	10.5:1	Direct Fuel Injection
Volkswagen TSI	DOHC	4	10.5:1	Direct Fuel Injection
Nissan DIG-S	DOHC	4	13.0:1	Direct Fuel Injection
PSA (group) PureTech	DOHC	4	10.5:1	Direct Fuel Injection
Renault Energy TCe 90	DOHC	4	9.5:1	Port Fuel Injection
Honda ECA Series 3-cyl.	SOHC	4	10.8:1	Port Fuel Injection
Toyota 1KR-FE	DOHC	4	10.5:1	Port Fuel Injection
Smart Fortwo	DOHC	4	11.4:1	Port Fuel Injection

Valve Train/Valves per Cylinder

Table 1.2 shows that, apart from one exception only, the most popular valve train is a **DOHC (double overhead camshaft)** valve train (Figure 1.4) with **4 valves per cylinder**.

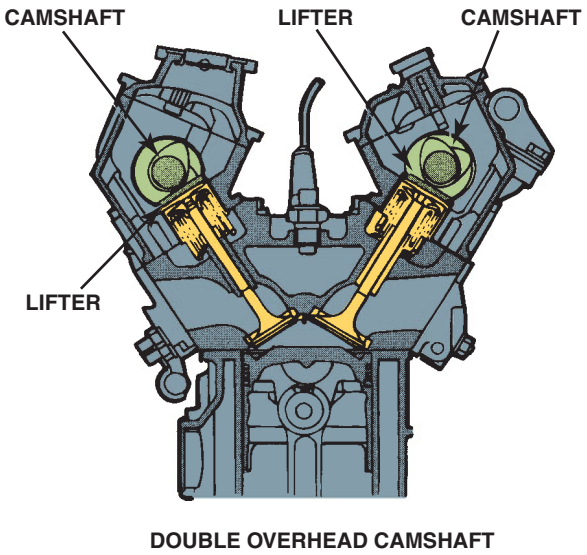

Figure 1.4. An example of a double overhead camshaft (DOHC) engine [6].

Compression Ratio

By analyzing the data from Table 1.2, the chosen **compression ratio** is **11.0:1**. This is an average value of all atmospheric engines that were analyzed.

Fuel Injection

Fuel injection presents a similar problem to air induction. Although the engine would benefit from having direct fuel injection, it would present the same problem as with choosing a turbocharger instead of natural aspiration. Being this an initial project, it must present a simple and inexpensive solution (as possible). Therefore, and since it is also a common choice for naturally aspirated engines, **port fuel injection** is chosen.

Summarizing, the engine's characteristics are:

- Four-Stroke
- Spark Ignition
- Inline three cylinder
- Four valves per cylinder
- Naturally Aspirated
- Port Fuel Injection
- DOHC – Double Overhead Camshaft
- 11.0:1 Compression Ratio

Apart from the compression ratio, the engine's characteristics are the same as Toyota's 1KR-FE engine. Therefore, this engine is used as a base/model whenever necessary.

2. ENGINE CYCLE

2.1. Overview

In any internal combustion engine, there is charge exchange in each engine cycle. On a 4-stroke SI engine, each cycle has, as the name indicates, four different strokes/phases (Figure 2.1).

"Engine cycles are identified by the number of piston strokes required to complete the cycle. A piston stroke is a one-way piston movement either from top to bottom or bottom to top of the cylinder. During one stroke, the crankshaft rotates 180° (1/2 revolution). A cycle is a complete series of events that continually repeats. Most automobile engines use a four-stroke cycle.

Intake stroke - The intake valve is open and the piston inside the cylinder travels downward, drawing a mixture of air and fuel into the cylinder. The crankshaft rotates 180° from top dead center (TDC) to bottom dead center (BDC) and the camshaft rotates 90° (top left of Figure 2.1).

Compression stroke - As the engine continues to rotate, the intake valve closes and the piston moves upward in the cylinder, compressing the air-fuel mixture. The crankshaft rotates 180° from bottom dead center (BDC) to top dead center (TDC) and the camshaft rotates 90° (top right of Figure 2.1).

Power stroke - When the piston gets near the top of the cylinder, the spark at the spark plug ignites the air-fuel mixture, which forces the piston downward. The crankshaft rotates 180° from top dead center (TDC) to bottom dead center (BDC) and the camshaft rotates 90° (bottom left of Figure 2.1).

Exhaust stroke - The engine continues to rotate, and the piston again moves upward in the cylinder. The exhaust valve opens, and the piston forces the residual burned gases out of the exhaust valve and into the exhaust manifold and exhaust system. The crankshaft rotates 180° from bottom dead center (BDC) to top dead center (TDC) and the camshaft rotates 90° (bottom right of Figure 2.1).

This sequence repeats as the engine rotates. To stop the engine, the electricity to the ignition system is shut off by the ignition switch, which stops the spark to the spark plugs. The combustion pressure developed in the combustion chamber at the correct time will push the piston downward to rotate the crankshaft. (…) Each cycle of events (four strokes) requires the engine crankshaft to make two complete revolutions, or 720° (360 × 2 = 720°). Each stroke of the cycle requires the crankshaft to rotate 180°. The greater the number of cylinders, the closer together the power strokes of the individual cylinders will occur." [6]. For an inline three-cylinder engine, the power strokes are separated by:

$$\frac{2\ \text{Complete Revolutions}}{\text{Number of Cylinders}} = \frac{360° \times 2}{3} = \frac{720°}{3} = 240° \tag{2.1}$$

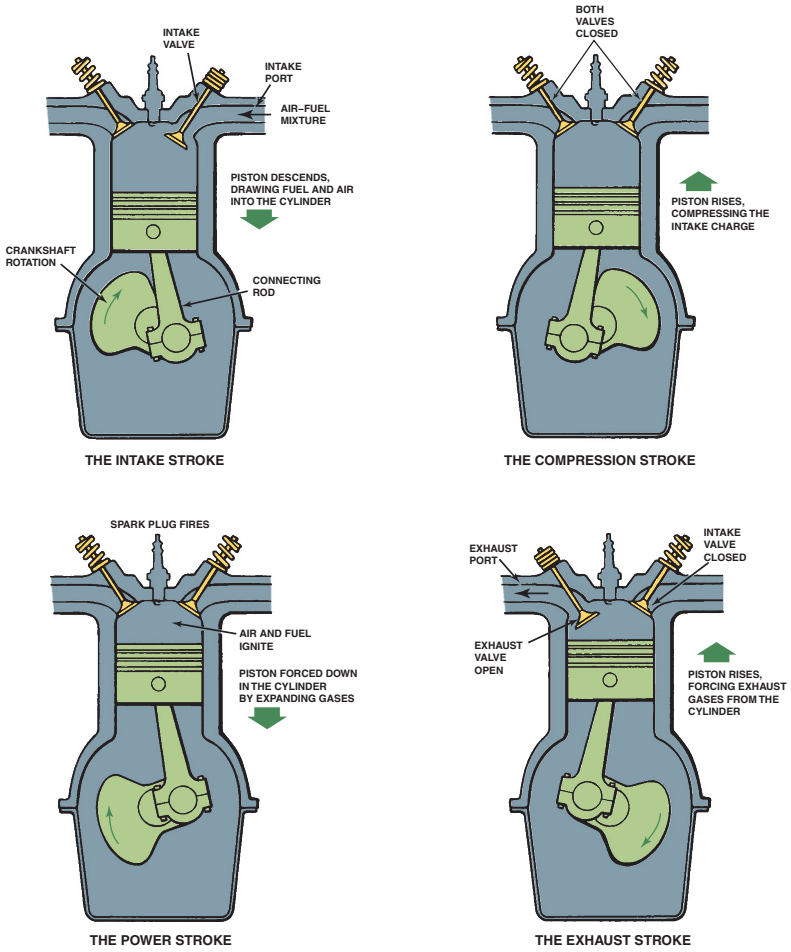

Figure 2.1. Four-stroke engine - Otto Cycle [6].

Having already defined the engine's characteristics (in Chapter 1) as well as the operating cycle's main aspects, the next step is to focus on the engine's operating cycle simulations. However, to begin them, the software has to undergo several modifications (the simpler modifications are explained on **Annex A**). Having been created around the PSA engine TU3JP-KFW with a 1.4-liter displacement and 2 valves per cylinder, many aspects that have direct influence on the program have to be modified, in order to create a version of the software that can accurately simulate the engine cycle of a 3-cylinder power unit with a 1.0-liter displacement.

One of the main aspects that needs to be addressed is the flame's behavior inside the combustion chamber. The combustion chamber of each engine is distinctively different. This aspect has a direct influence in the flame's behavior inside the chamber. Because the program relies on the flame's behavior to work, it is necessary to adapt the software to this particular situation. Therefore, a new combustion chamber must be designed and the flame behavior inside it analyzed.

2.2. Combustion Chamber

2.2.1. Overview

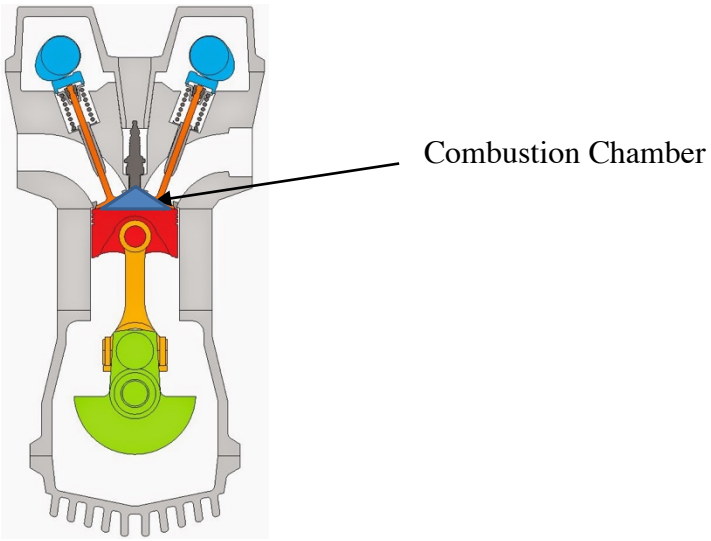

Figure 2.2. Schematic example of an ICE (internal combustion engine) combustion chamber (represented as the blue triangle) [7].

As depicted in Figure 2.2, the engine's combustion chamber is defined as the volume between the cylinder head and the piston at TDC (top dead center). An efficient

combustion chamber is absolutely central for obtaining the highest possible brake power (P_b) with the lowest possible brake specific fuel consumption (bsfc).

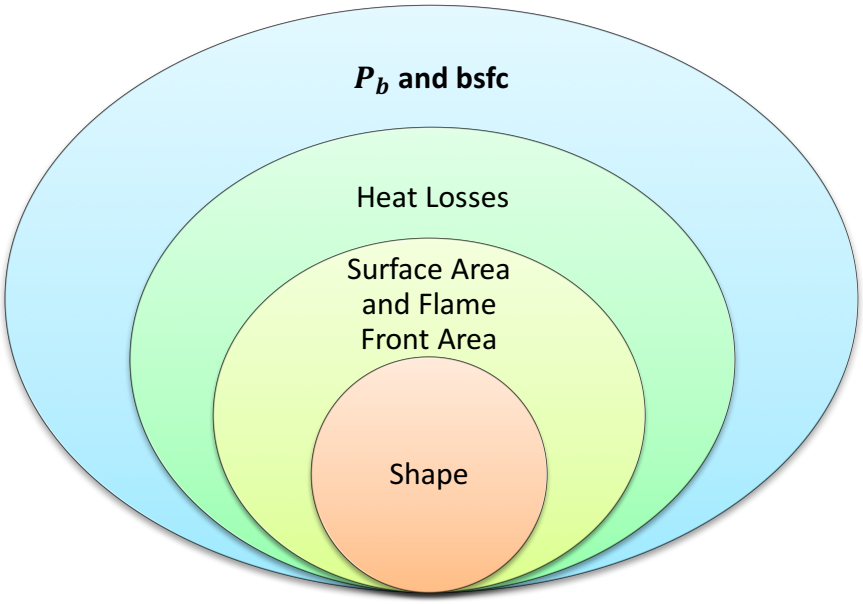

Figure 2.3. Venn diagram explaining how the chamber's shape affects its efficiency.

An accurate assessment of the combustion chamber's shape (Figure 2.3) is a key element to obtain good results. To successfully design the combustion chamber, two main variables need to be accounted for: The volume of the chamber and its surface area.

2.2.2. Volume

In order to calculate the chamber's volume, it is necessary to know the cylinder displacement volume, V_{dc},which is given by Equation (2.2):

$$V_{\mathrm{dc}} = \frac{V_d}{n_{\mathrm{cyl}}} = \frac{1000\ \mathrm{cm}^3}{3} = 333.33\ \mathrm{cm}^3 \tag{2.2}$$

Where:

V_d – Engine displacement volume;

n_{cyl} – Number of cylinders;

With the cylinder displacement volume and the compression ratio, r_c, it is now possible to determine the **volume of the combustion chamber**, V_{c}, with Equation (2.3).

$$V_{\mathrm{c}} = \frac{V_{\mathrm{dc}}}{r_c - 1} = \frac{333.33\ \mathrm{cm}^3}{11 - 1} = 33.33\ \mathrm{cm}^3 \tag{2.3}$$

2.2.3. Design

In Autodesk Inventor 2016, it is possible to design the combustion chamber with the previously calculated volume of 33.33 cm^3. As was already defined, the engine will house a DOHC valve train. Therefore, a pent-roof combustion chamber must be designed. To create the combustion chamber, a base model is needed. Since Toyota's 1KR-FE engine also has a pent-roof combustion chamber, the first step is to design it as close as possible to the one used on the "model" engine (Figure 2.4).

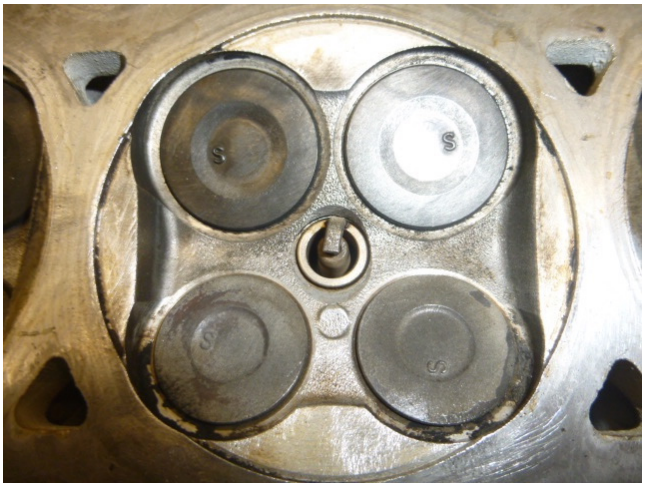

Figure 2.4. 1KR-FE Engine's cylinder head [8].

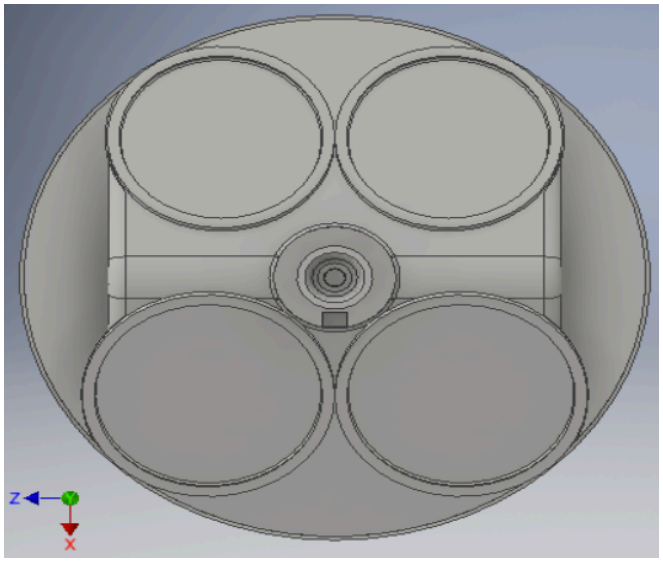

Figure 2.5. 1KR-FE Engine's combustion chamber (designed in Autodesk Inventor 2016).

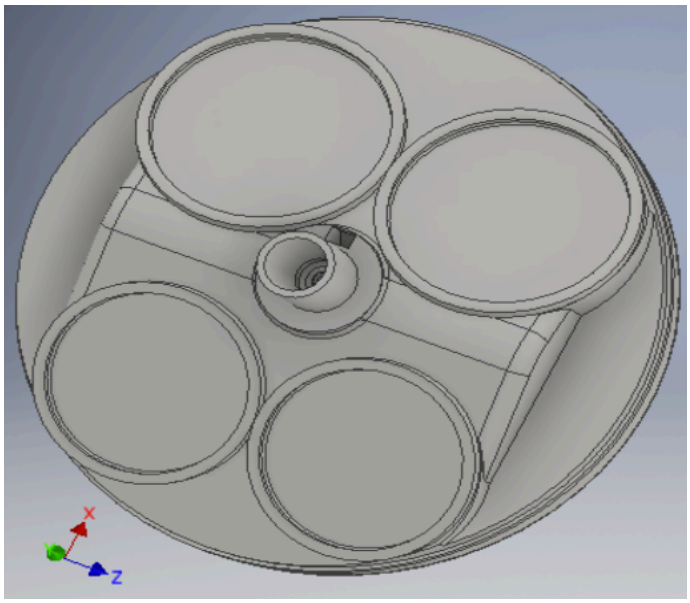

Figure 2.6. 1KR-FE Engine's combustion chamber (designed in Autodesk Inventor 2016).

As shown in Figure 2.5, the combustion chamber is designed as a solid volume, much like a "negative" from a photograph. After the first chamber design is completed (Figure 2.5 and Figure 2.6), it is possible to begin the optimization process, as there is clearly room for improvement.

The engine cycle simulation software is used to evaluate the optimization process and determine which combustion chamber shape is better. The combustion chamber's area plays an essential role in the software's calculation of heat losses. The program measures the heat losses through two coefficients - K_{ch} and K_{p}:

$$K_{\mathrm{ch}} = \frac{\text{Surface Area of the Cylinder Head}}{\text{Cylinder Cross Section Area}} \tag{2.4}$$

$$K_{\mathrm{p}} = \frac{\text{Surface Area of the Piston Crown}}{\text{Cylinder Cross Section Area}} \tag{2.5}$$

Before and after each optimization, both cylinder head and piston crown surface areas are measured (the cylinder's cross-section area is constant since the bore is also constant). Those measurements are inserted on K_{ch} and K_{p} coefficients which immediately changes the engine's P_b and bsfc values. The ultimate purpose of the optimization is to obtain

the highest possible P_b value and the lowest possible bsfc value. This is attained by reducing the heat losses. The optimization methodology is explained in Figure 2.7:

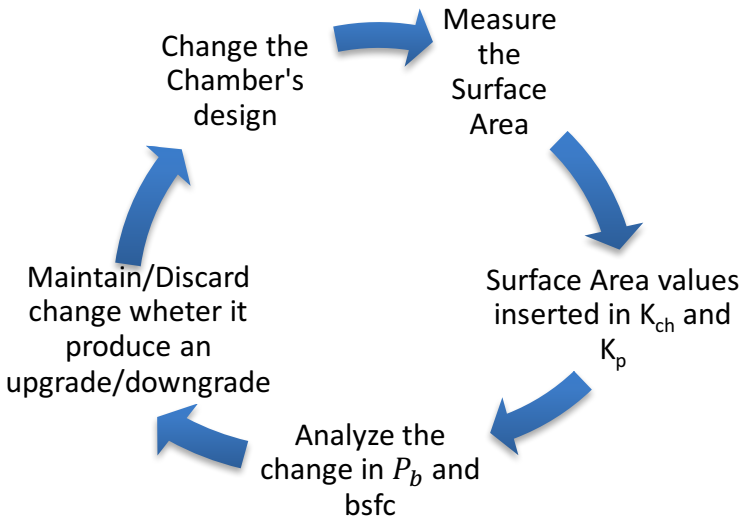

Figure 2.7. Iterative process for the combustion chamber's optimization.

The current shape of the chamber's top end favors turbulence, especially at the end of the compression stroke. Although this is an advantage, the absence of material on the top sides (left and right side of Figure 2.5), and also its complicated shape, bring up two significant problems to the combustion chamber. In the first place, it increases the chamber's surface area, which leads to significant **heat losses**. On second place, it creates the need to increase the chamber's convex bottom - in order to comply with the previously calculated volume of the combustion chamber. A greater volume on the inferior side of the chamber (Figure 2.8 and Figure 2.9) is a synonym of an equally greater cavity on the piston head, which would lead to a more complex piston manufacture.

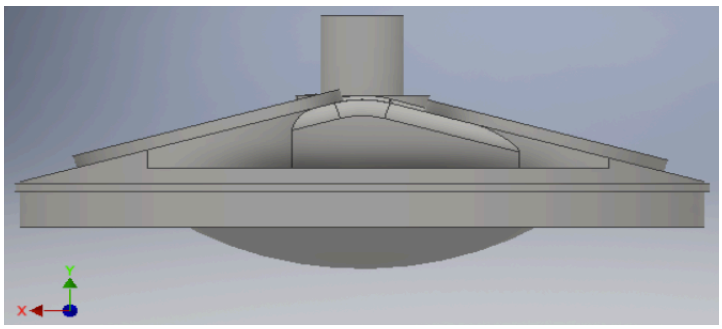

Figure 2.8. 1KR-FE Engine's combustion chamber – lateral view (designed in Autodesk Inventor 2016).

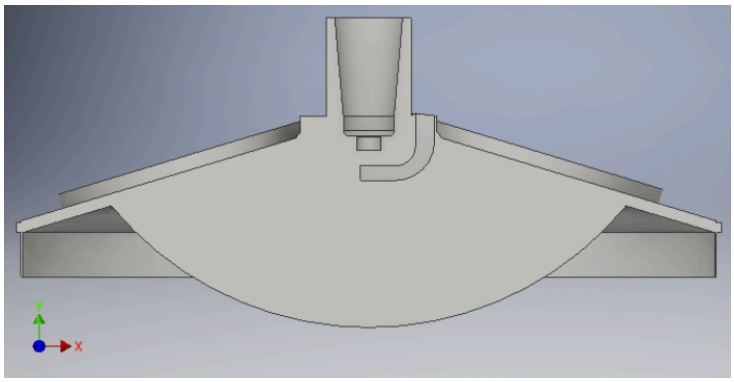

Figure 2.9. 1KR-FE Engine's combustion chamber – cutaway view (designed in Autodesk Inventor 2016).

After several iterations, it is possible to obtain an optimized solution (Figure 2.10). Starting with the chamber's top half, volume is added to both sides, producing a much more homogeneous design. With these changes, the surface area is diminished and the heat losses minimized. The changes on the chamber's top end also help to improve its bottom half. By adding volume to the top, it is possible to reduce the convex bottom of the chamber (3 millimeters less in height), which means a better solution for the piston's design and manufacture, while still maintaining the previously calculated chamber volume (Figure 2.11 and Figure 2.12). The improvements also include shortening the extrusions that surrounded the spark plug and the valves to the minimum possible height.

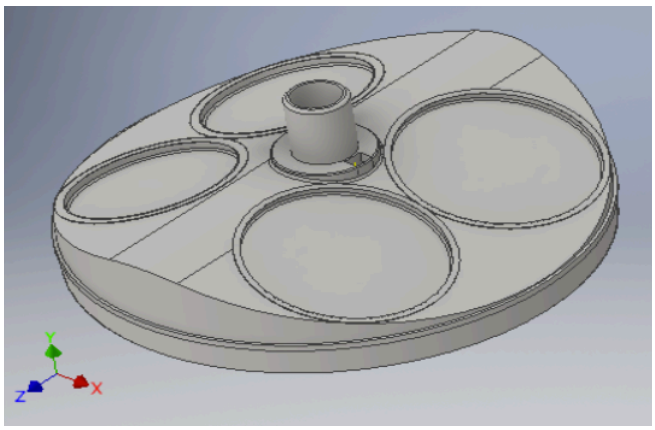

Figure 2.10. Optimized final solution of the combustion chamber (designed in Autodesk Inventor 2016).

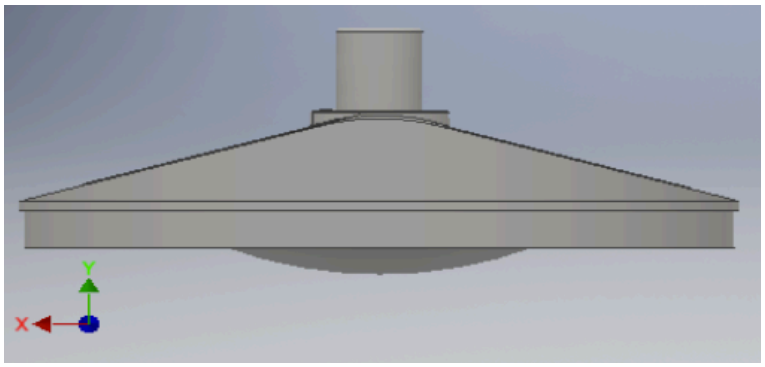

Figure 2.11. Optimized final solution of the combustion chamber – lateral view (designed in Autodesk Inventor 2016).

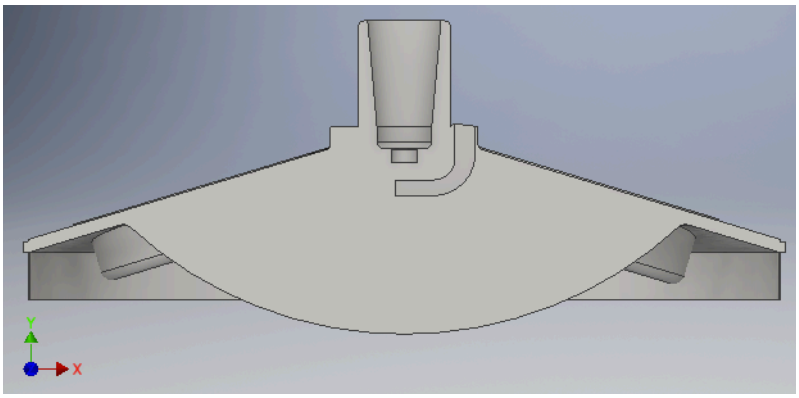

Figure 2.12. Optimized final solution of the combustion chamber – cutaway view (designed in Autodesk Inventor 2016).

With the optimization process complete, it is possible to conclude that the final shape is capable of delivering brake power with a lower bsfc, and, for that reason, is a better solution than the initial one. It is also possible to conclude that, although the first combustion chamber has the advantage of creating more turbulence at the end of the compression stroke, that fact does not compensate for its greater heat losses.

2.2.4. Flame Behavior Throughout the Combustion Chamber

With the combustion chamber's design concluded, it is possible to evaluate the flame's behavior throughout the chamber. To do this, a technique developed in [9] is used on Autodesk Inventor 2016. This technique consists of designing and extruding a sphere inside the combustion chamber. The sphere has its center placed on the middle of the spark plug's electrodes and represents the volume of the flame that is burning inside the chamber. The process is started with a small sphere diameter, which is incrementally increased throughout. When extruding the sphere, the combustion chamber and the sphere intersect

each other, forming a surface (Figure 2.13). This surface is the flame front. Following the same procedure as [9], there are two ways of measuring the flame front's surface. The first one is used as long as the flame front's surface isn't touching the combustion chamber's walls. It consists of only extruding the volume that is contained inside the flame front's surface and measuring its outside area (left of Figure 2.13). The second one is used from the point where the flame front touches the chamber's wall onwards. In this situation, the measurement procedure is adapted. The volume contained inside the flame front's surface is eliminated and the remaining volume of the chamber is maintained. The blue surface on the right hand side of Figure 2.13 represents the flame front's surface area that is measured.

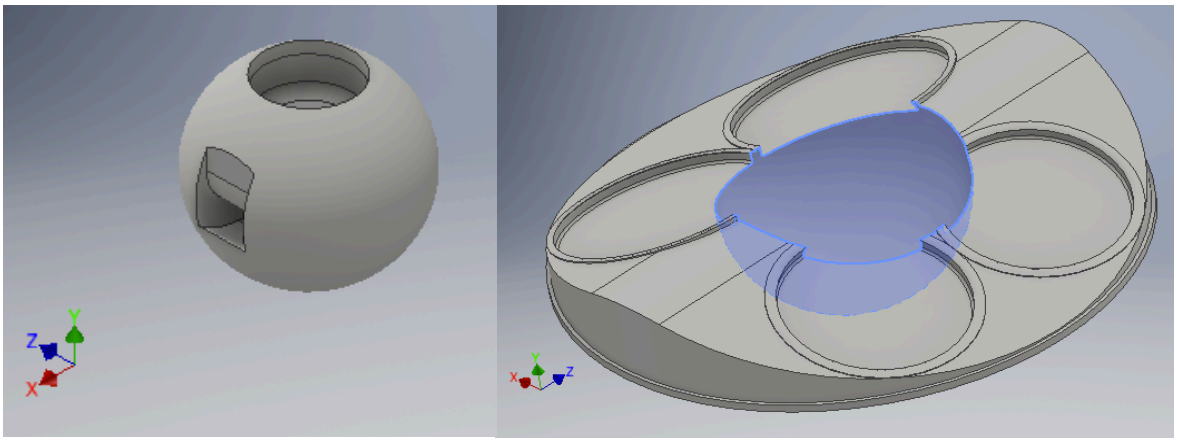

Figure 2.13. Intersection between the sphere and the combustion chamber. This intersection represents the flame front's surface area (designed in Autodesk Inventor 2016).

A_b, which is the flame front's surface area, is determined by measuring the intersection's surface. By incrementally increasing the diameter of the sphere, it is possible to evaluate the growth of the flame front's surface area throughout the combustion process. However, to perform this evaluation, an assumption has to be made. It is assumed that the combustion chamber has a constant geometry. The considered geometry is the one it has when the piston is at TDC (Figure 2.14). It is also necessary to suppress the "skirt" around the combustion chamber to obtain accurate results (Figure 2.15). This "skirt" represents the clearance volume between the piston and the cylinder above the first compression ring. In reality, the mass contained by the "skirt" is very small and therefore has no significant contribution to the heat losses. However, if it was to be considered, it would significantly increase the surface area and cause the calculated heat losses to be much higher than what they actually are.

Figure 2.14. Schematic example of a combustion chamber with the piston at TDC [10].

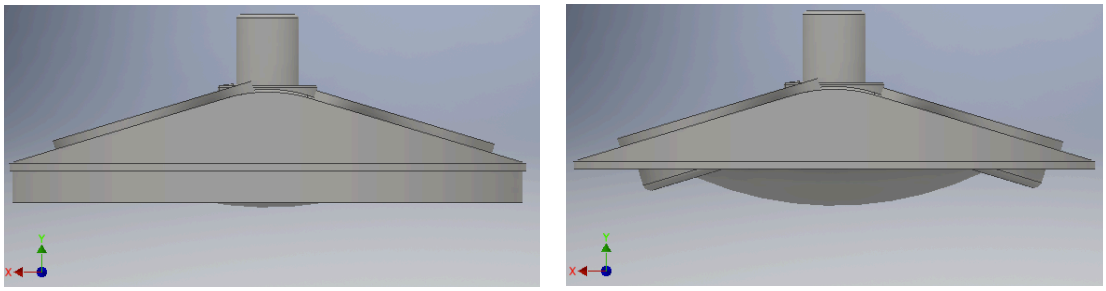

Figure 2.15. Combustion chamber with (left) and without (right) "skirt" (designed in Autodesk Inventor 2016).

With all of the measurements completed, it is possible to perform a polynomial fit and obtain the results depicted in Figure 2.16. The presented equation on Figure 2.16 expresses the relation between V_b/V_c and r_b/B.

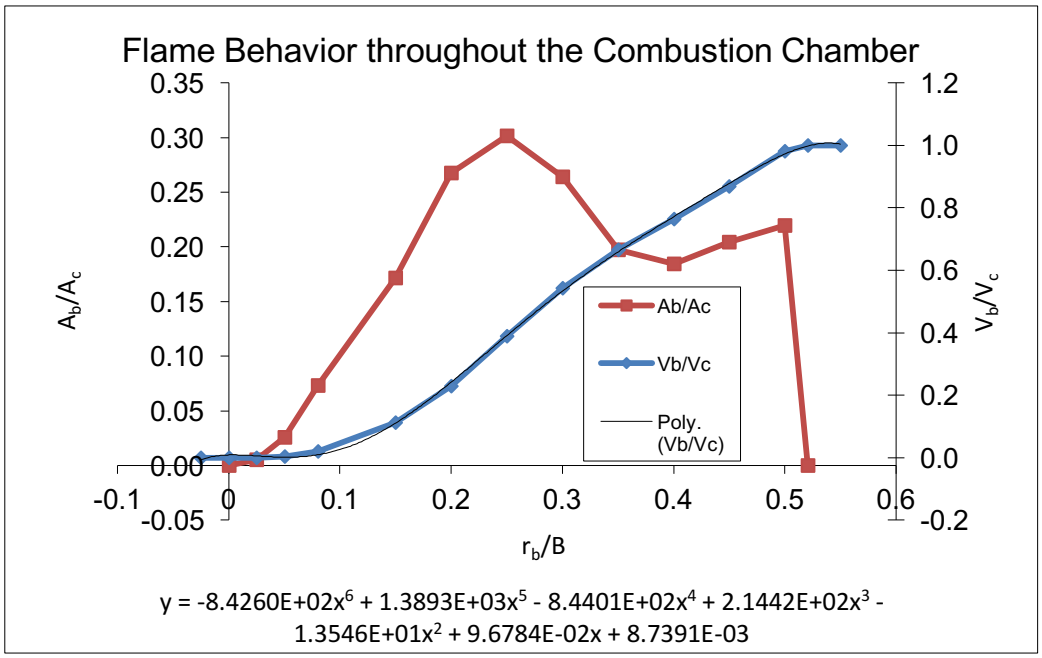

Figure 2.16. Flame behavior throughout the combustion chamber.

Being:

- A_b/A_c – Flame front surface area/Cylinder cross section area;
- V_b/V_c – Volume burned/Combustion chamber volume;
- r_b/B – Burned gas radius/Cylinder bore

The curves depicted in Figure 2.16 illustrate the flame's behavior inside the combustion chamber. From the red curve it is possible to conclude that A_b/A_c has a steady growth until $r_b/B = 0.25$. After this point the curve shows some significant fluctuations. This is due to the shape of the combustion chamber's top and the increasing value of r_b/B. V_b/V_c (shown by the blue curve) has a steady growth throughout this analysis.

2.3. Engine Cycle Simulations

2.3.1. Overview

With all software modifications done, it is now possible to simulate the engine's operating cycle. The cycle is simulated using a program developed at DEM-FCTUC on Microsoft Office Excel [1] (Figure 2.17).

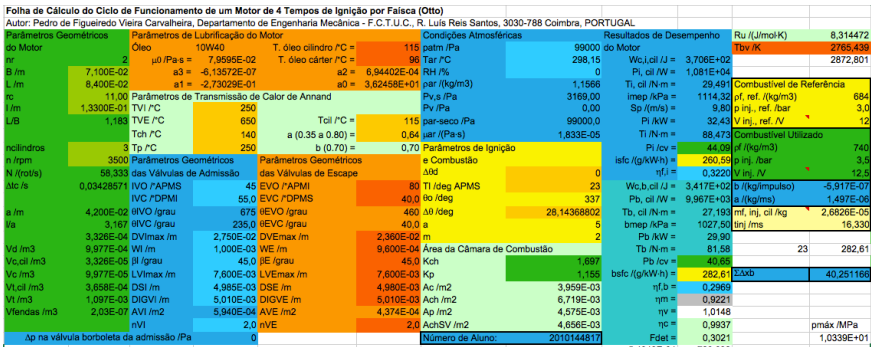

Figure 2.17. Overview of the engine's cycle simulation program [1].

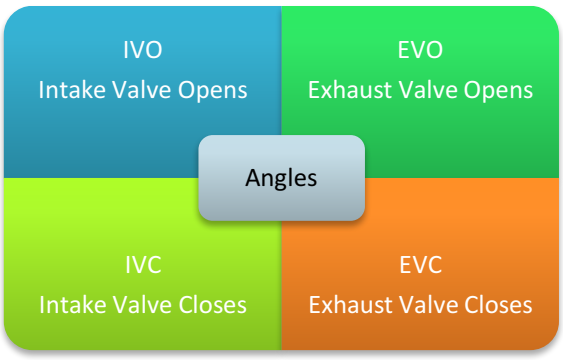

Figure 2.18. The four angles to be determined through engine cycle simulation.

Both intake and exhaust valves play a very important role on each stroke of the engine's cycle. By simulating the engine's operating cycle, it is possible to define two main aspects of both the engine cycle and the valve train:

1. The optimal opening and closing angles of both intake and exhaust valves (Figure 2.18), as a function of the engine's rotation speed at maximum torque;
2. The optimal lift of both intake and exhaust valves, as a function of load and the engine's rotation speed;

All simulations are carried out with stoichiometric air-fuel mixture because the engine is intended for a three-way catalyst exhaust gas after treatment. The opening and closing angles are the first aspect to be addressed. It is necessary to determine all four angles (Figure 2.18) throughout the engine's operating range. In order to cover this range, some fixed n values are established. The chosen values of n are based on these factors:

1. *n* for expected maximum power: 6000 rpm, based on the data obtained from the 1KR-FE engine (Figure 2.19);
2. *n* for expected maximum torque: 3500 rpm, based on the data obtained from the 1KR-FE engine (Figure 2.19);
3. *n* values to cover the engine's operating range: 1500 rpm, 5000 rpm;

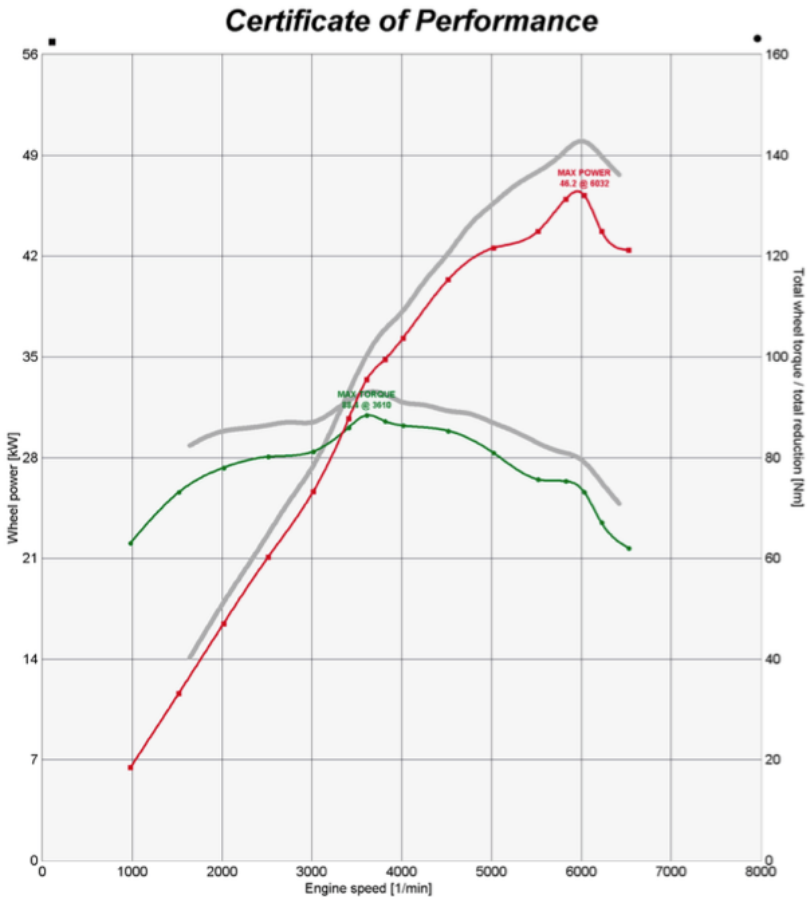

Figure 2.19. 1KR-FE's "Certificate of Performance" showing the maximum power and torque for the engine's operating range [11].

2.3.2. Intake and Exhaust Valves Optimal Opening and Closing Angles

2.3.2.1. Methodology

It is necessary to test different methodologies in order to establish the best possible iterative process to find the optimal values of all four angles. Initially, the ignition timing (TI) is kept constant throughout the process and the optimal value of each angle is chosen according to the **lowest brake specific fuel consumption criterion**. It consists of choosing the angles and ignition timing which provide the engine with the lowest possible bsfc. The first methodology is composed of the following steps:

1. An initial value for each angle is chosen (as close as possible to the expected value);

2. The program is run with the initial four angle combination in order to find the optimal value of TI with the lowest bsfc criterion;

3. Once the optimal value of TI is established, the program is run with different values of the IVO angle (positive and negative increments of five degrees). The optimal IVO angle is established while the other three angles remain constant;

4. After obtaining the optimal angle for the IVO, the same process is applied for the IVC angle, however, now the program is run with the new IVO angle on the four angle combination;

5. The process is repeated for the EVO and EVC angles;

This methodology has three important flaws. The first one is that it establishes the optimal value of TI at the start and keeps it constant throughout the process. Due to this procedure, the optimal value of TI is only correctly applied for the first combination of angles. As soon as the IVO angle changes, the ignition timing is already outdated. It is therefore necessary to update the TI value throughout the process. The second flaw is that this methodology only relies on one criterion to determine the optimal angles – the lowest brake specific fuel consumption. It is also necessary to analyze whether other criterion could produce a better result. The **highest brake power criterion** must be tested. It consists of selecting the angles and timing ignition which provide the engine with the highest possible brake power. The last important flaw of this process is that it depends heavily on the initial four angle combination. Therefore, it is mandatory to perform a second round of iteration to minimize the angle combination's influence.

By correcting the previous flaws, the desired methodology is achieved:

1. An initial value for each angle is chosen (as close as possible to the expected value);

2. The program is run with the initial four angle combination in order to find the (initially) optimal angle of TI with the lowest bsfc criterion;

3. Once the optimal angle of TI is established, the program is run with different variations of the IVO angle (positive and negative increments of five degrees). For each variation of the IVO angle, the optimal value of TI is determined. The optimal angles of IVO and TI are established while the other three angles remain constant;

4. After obtaining the optimal IVO and TI angles, the same process is applied for the IVC angle, however, now the program is run with the new value of IVO on the four angle combination;

5. The process is repeated for the EVO and EVC angles;

6. The process is repeated for the highest brake power criterion;
7. A second iteration of the process with each criteria is performed;

All engine cycle simulations that are carried out to determine the optimal opening and closing angles of both intake and exhaust valves are performed at wide open throttle (WOT) and have a constant valve lift of 0.0076 m on both intake and exhaust valves. This value is taken from the "model" engine.

2.3.2.2. Highest Brake Power Criterion

Table 2.1. Highest brake power criterion results.

n [rpm]	P_b [kW]	bsfc [g/kW·h]	IVO [°]	IVC [°]	EVO [°]	EVC [°]
1500	13.60	266.88	20	15	40	15
3500	33.35	259.49	30	30	60	25
5000	45.86	265.74	30	45	70	30
6000	52.32	272.76	35	55	75	35

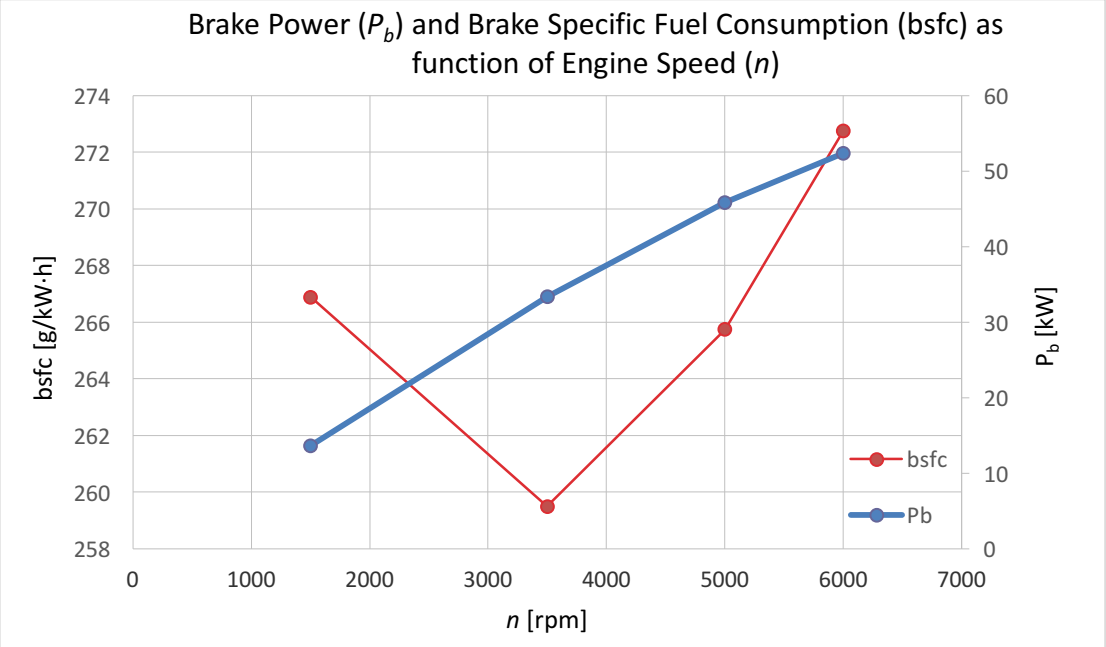

Figure 2.20. Evolution of engine brake power and brake specific fuel consumption throughout the engine's operating range for a valve lift of 0.0076 m on both intake and exhaust valves at WOT.

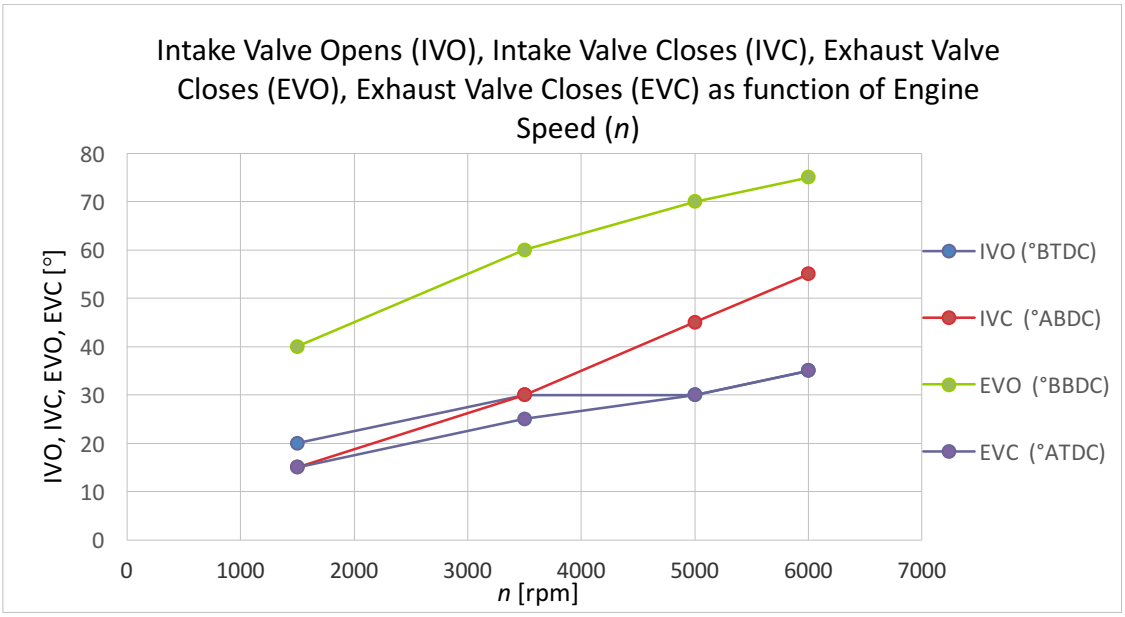

Figure 2.21. Intake and exhaust valves opening and closing angles throughout the engine's operating range for a valve lift of 0.0076 m on both intake and exhaust valves at WOT.

Lowest bsfc criterion

Table 2.2. Lowest bsfc criterion results.

n [rpm]	P_b [kW]	bsfc [g/kW×h]	IVO [°]	IVC [°]	EVO [°]	EVC [°]
1500	-	-	-	-	-	-
3500	33.13	259.46	40	35	60	30
5000	45.46	265.42	45	45	75	35
6000	52.02	272.36	45	55	80	40

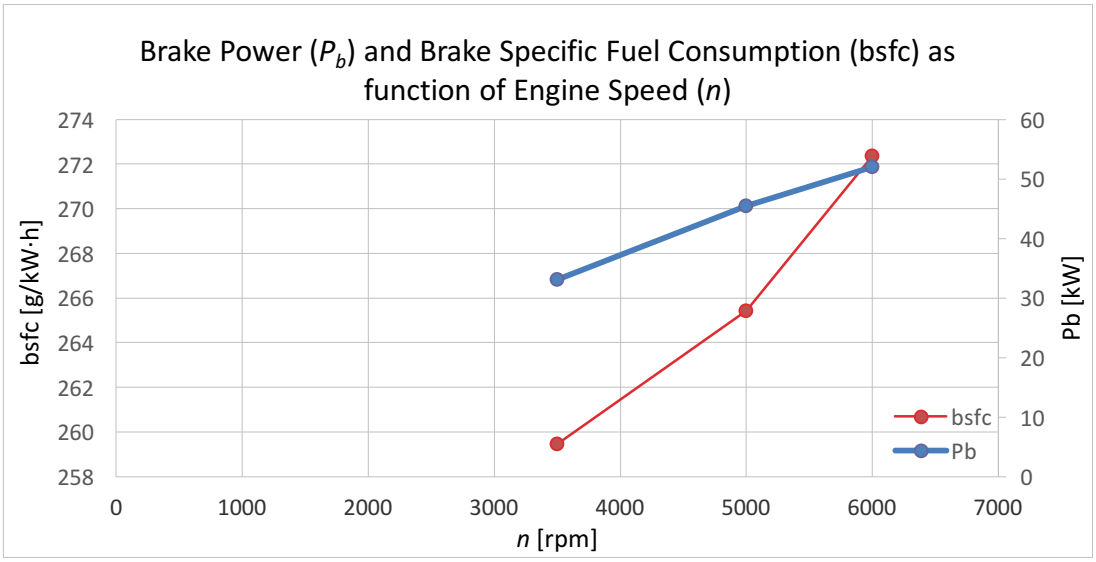

Figure 2.22. Evolution of engine brake power and brake specific fuel consumption throughout the engine's operating range for a valve lift of 0.0076 m on both intake and exhaust valves at WOT.

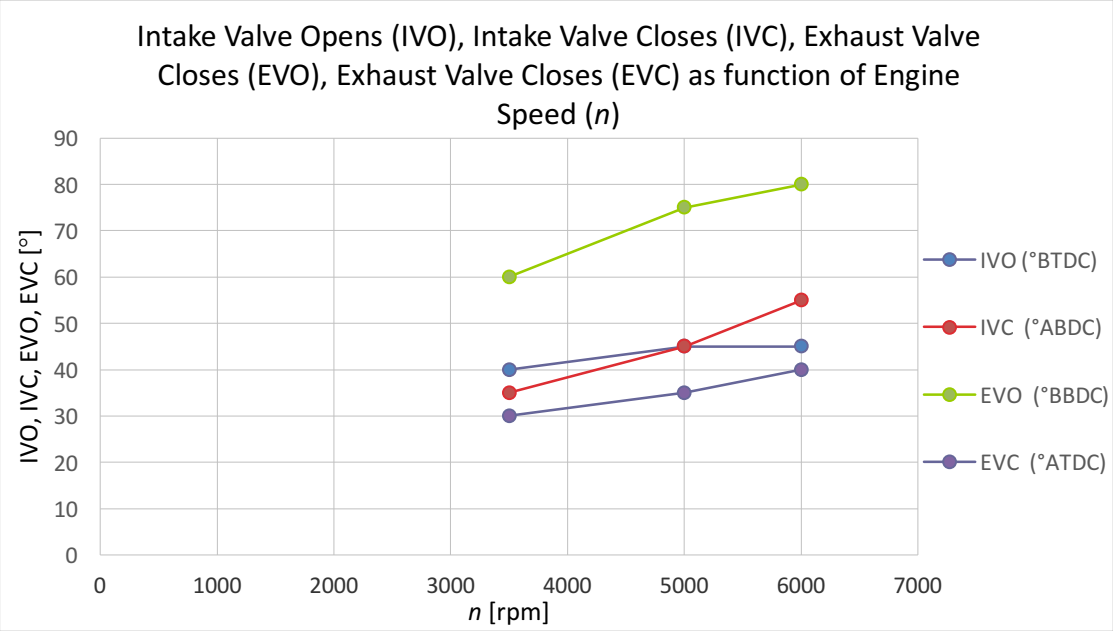

Figure 2.23. Intake and exhaust valves opening and closing angles throughout the engine's operating range for a valve lift of 0.0076 m on both intake and exhaust valves at WOT.

By analyzing the final results of both criteria, it can be concluded that the highest brake power (Table 2.1) produces the best results (Figure 2.20 and Figure 2.21). The gain in brake power from this criterion compensates the small increase in bsfc. With the lowest brake specific fuel consumption criterion (Table 2.2), the fuel savings do not compensate for the loss in brake power (Figure 2.22). Furthermore, the brake power criterion also leads to smaller opening and closing angles.

2.3.3. Intake Valves Optimal Lift

2.3.3.1. Methodology

With the angles determined, it is necessary to analyze the lift of both intake and exhaust valves. Until this point, the valve lift was considered constant (0.0076 m) for both intake and exhaust valves. As was already mentioned, variable valve lift can enhance brake power and lower both brake specific fuel consumption and emission levels. The implementation of variable valve lift on an internal combustion engine suppresses the need for a butterfly throttle valve.

"In a gasoline engine, the speed and power are controlled by the throttle valve, which controls the amount of air entering the engine. Adding more fuel to the cylinders of a

gasoline engine without adding more air (oxygen) will not increase the speed or power of the engine." [6].

It's typical for an SI engine to operate with a butterfly throttle valve, also known as a throttle, which is located in the engine's intake manifold. While the driver controls the vehicle's acceleration using the throttle pedal, the throttle valve accordingly regulates the amount of air entering the engine. Consequently, the amount of fuel that enters the engine is controlled by the ECU in accordance to the air allowed in by the throttle. The problem of having a throttle valve in the intake manifold is that it induces pumping losses. Pumping losses are estimated to be 10% of the total losses in conventional SI engines equipped with a butterfly throttle valve. Variable intake valve lift is an alternative to the butterfly valve.

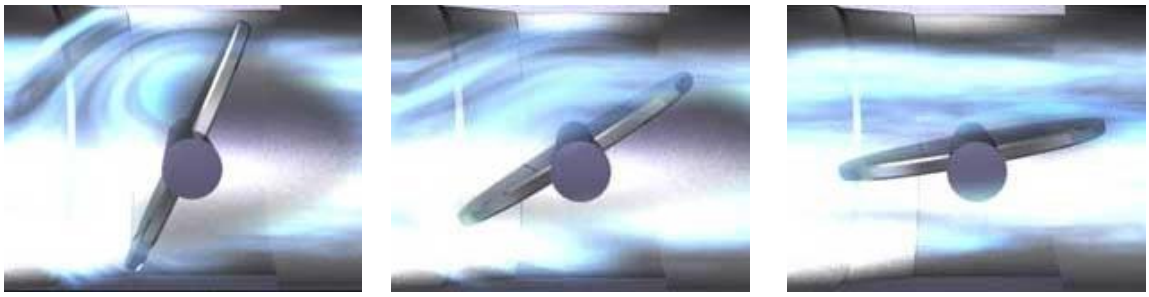

Figure 2.24. Effect of the butterfly throttle valve. Position from left to right: Idle; Partial Load; Full Load [12].

With variable intake valve lift, the amount of air entering the engine can be controlled directly by the higher or lower lift of the intake valves, without the need for a butterfly throttle valve. Although the pressure loss still exists, there is a clear advantage in regulating the air intake with valve lift instead of using a butterfly throttle valve. In partial load the butterfly valve is semi-closed (central image of Figure 2.24), whereas with variable intake valve lift the intake valves produce a smaller lift. For the same pumping loss of the butterfly throttle valve, variable intake valve lift increases turbulence intensity and reduces Kolmogorov's turbulence scale. This leads to an increase in burning rate and to a reduction in burning time. The engine produces more work with the same amount of fuel-air mixture, which reduces bsfc at part load to a maximum of about 10%.

Obviously, the implementation of variable valve lift has higher costs than simply including a butterfly throttle valve. Therefore, the difference in bsfc of both situations must be analyzed in order to evaluate if this technology is worth the extra cost.

2.3.3.2. Results

Once again, the engine cycle simulation program is used. The chosen rotation is n = 3500 rpm. Besides being an intermediate value of engine speed, it is also the one with the lowest bsfc value. Initially, the butterfly throttle valve is simulated with different values of total pressure loss: 15000 Pa, 30000 Pa and 45000 Pa. For each value of total pressure loss, the optimal value of TI is determined. The butterfly throttle valve simulations are performed with a constant valve lift of 0.0076 m for both intake and exhaust valves.

The next step is to analyze the variable valve lift on the intake side. To accurately compare both systems – and since the different values of total pressure loss are not applicable in this situation – bmep (brake medium effective pressure) values need to be matched. To accomplish this, the intake valve lift needs to be adjusted (Table 2.3). The exhaust valve lift is kept constant, and, once again, the optimal value of TI is determined with the engine cycle simulations (Table 2.4).

Table 2.3. Variable intake valve lift.

bmep [kPa]	Intake Valve Lift [m]	Exhaust Valve Lift [m]
1146	0.007600	0.0076
1135	0.006800	0.0076
1061	0.005000	0.0076
883	0.003660	0.0076
634	0.002710	0.0076
389	0.001950	0.0076
226	0.001431	0.0076
0	0.000675	0.0076

Table 2.4. Comparison between Butterfly Throttle Valve (BTV) and Variable Valve Lift (VVL) (on intake only) for an n = 3500 rpm.

	Total Pressure Loss [Pa]	bmep [kPa]	TI [°BTDC]	bsfc [g/kW·h]	T_b [N·m]
BTV	15000	883	22	275.37	70.13
VVL		883	13	273.74	70.10
BTV	30000	634	29	303.59	50.32
VVL		634	13	297.85	50.36
BTV	45000	389	42	367.79	30.86
VVL		389	14	348.21	30.90
BTV	55000	226	62	489.35	17.94
VVL		226	15	437.76	17.95

Being:

BTV – Butterfly Throttle Valve

VVL – Variable Valve Lift (intake only)

T_b – Brake Torque [N·m]

Table 2.3 also shows another important fact. If we analyze the evolution of bmep as a function of intake valve lift (Figure 2.25) it is obvious to state that the bmep gain above 0.0076 m is minimal. 0.0076 m is therefore a good value to take as maximum intake valve lift.

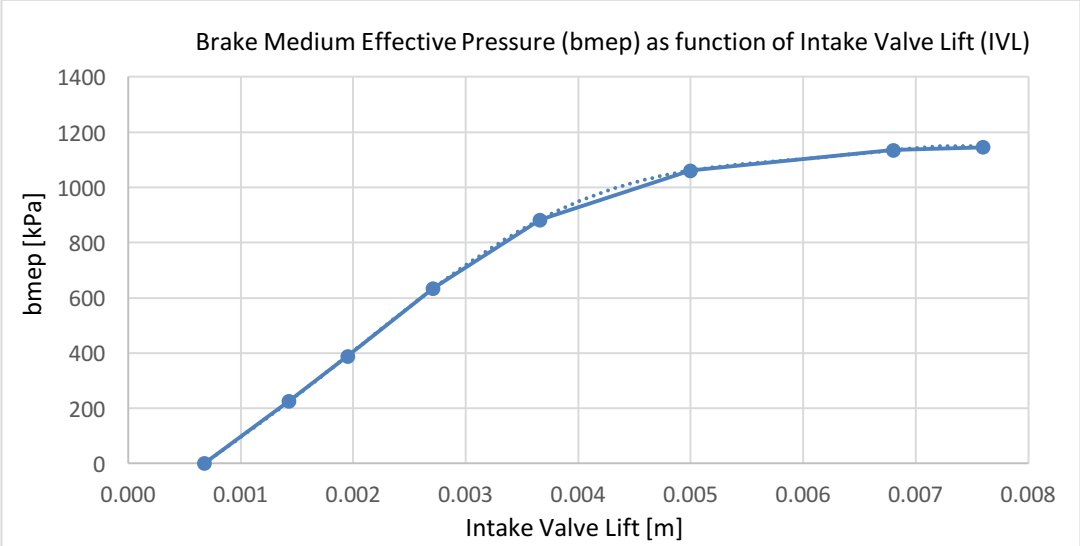

Figure 2.25. Evolution of bmep as function of (IVL) for n = 3500 rpm.

2.3.4. Exhaust Valves Optimal Lift

2.3.4.1. Methodology

The final step in terms of engine cycle simulations is to analyze the effect of exhaust valve lift on bsfc. The exhaust valve lift was changed from 0.006 m to 0.01 m, for a constant intake valve lift and the effect on bsfc was evaluated.

2.3.4.2. Results

The results for an intake valve lift equal to 0.00366 m are presented in Table 2.5 and Figure 2.26.

Table 2.5. Evolution of bsfc with EVL and a constant IVL = 0.00366 m.

n [rpm]	Exhaust Valve Lift [m]	TI [°BTDC]	bsfc [g/kW·h]	T_b [N·m]
3500	0.0100	13	273.51	70.18
3500	0.0090	13	273.54	70.17
3500	0.0085	13	273.58	70.16
3500	0.0080	13	273.66	70.13
3500	0.0076	13	273.74	70.10
3500	0.0070	13	273.93	70.03
3500	0.0060	13	274.56	69.80

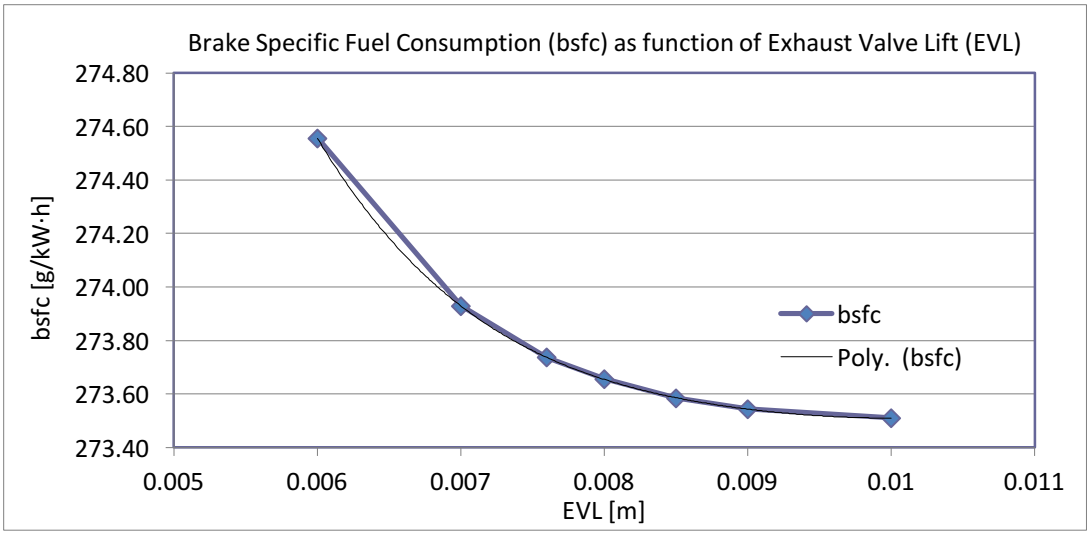

Figure 2.26. Evolution of bsfc with EVL and a constant IVL = 0.00366 m.

The results for an intake valve lift equal to 0.00271 m are presented in Table 2.6 and Figure 2.27.

Table 2.6. Evolution of bsfc with EVL and a constant IVL = 0.00271 m.

n [rpm]	Exhaust Valve Lift [m]	TI [°BTDC]	bsfc [g/kW· h]	T_b [N· m]
3500	0.0100	13	297.63	50.42
3500	0.0090	13	297.66	50.41
3500	0.0085	13	297.70	50.40
3500	0.0080	13	297.76	50.38
3500	0.0076	13	297.85	50.36
3500	0.0070	13	298.03	50.31

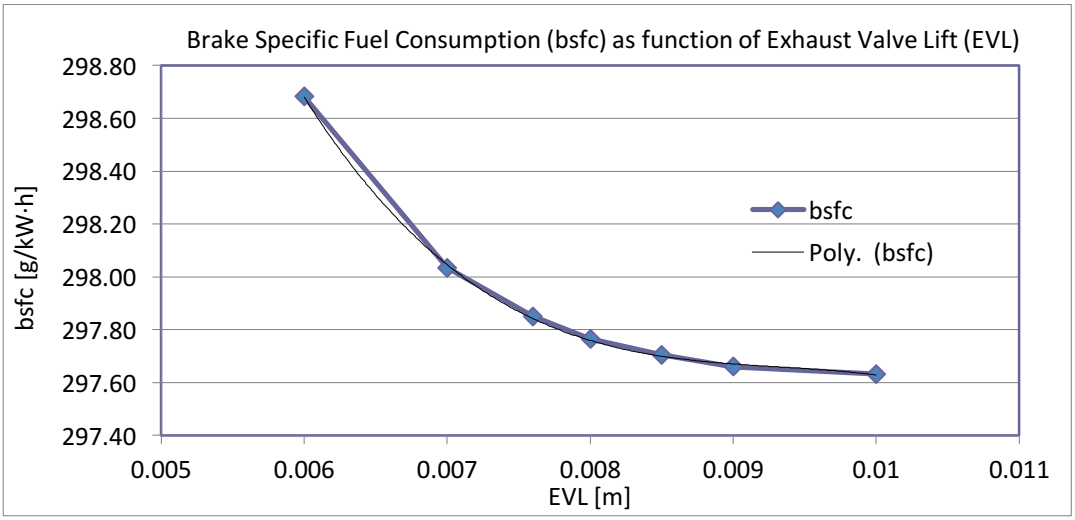

Figure 2.27. Evolution of bsfc with EVL and a constant IVL = 0.00271 m.

The results for an intake valve lift equal to 0.00195 m are presented in Table 2.7 and Figure 2.28.

Table 2.7. Evolution of bsfc with EVL and a constant IVL = 0.00195 m.

n [rpm]	Exhaust Valve Lift [m]	TI [°BTDC]	bsfc [g/kW· h]	T_b [N· m]
3500	0.0100	14	347.78	30.96
3500	0.0090	14	347.87	30.95
3500	0.0085	14	347.95	30.94
3500	0.0080	14	348.07	30.92
3500	0.0076	14	348.21	30.90

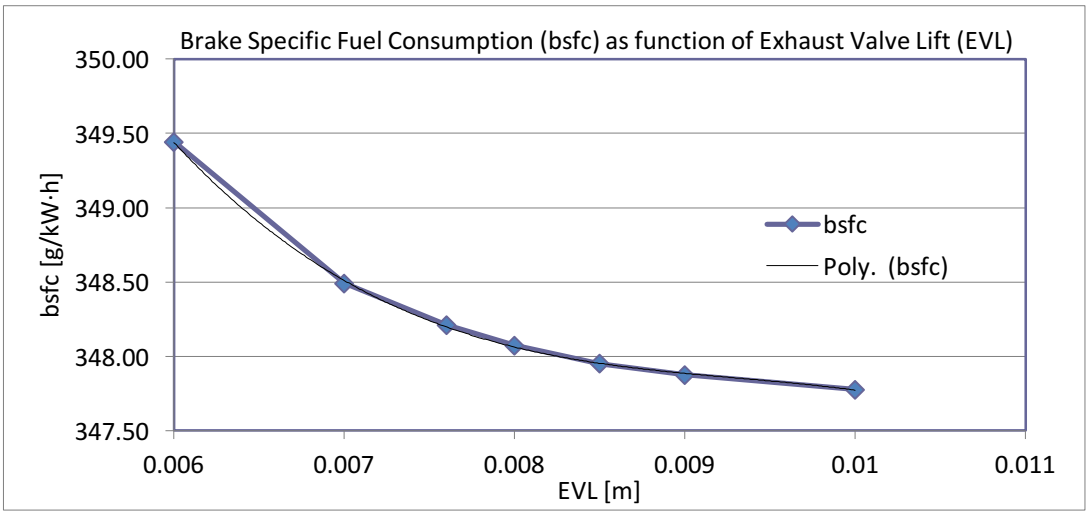

Figure 2.28. Evolution of bsfc with EVL and a constant IVL = 0.00195 m.

The results for an intake valve lift equal to 0.00143 m are presented in Table 2.8 and Figure 2.29.

Table 2.8. Evolution of bsfc with EVL and a constant IVL = 0.00143 m.

n [rpm]	Exhaust Valve Lift [m]	TI [°BTDC]	bsfc [g/kW·h]	T_b [N·m]
3500	0.0100	15	436.41	18.02
3500	0.0090	15	436.80	18.00
3500	0.0085	15	437.06	17.99
3500	0.0080	15	437.40	17.97

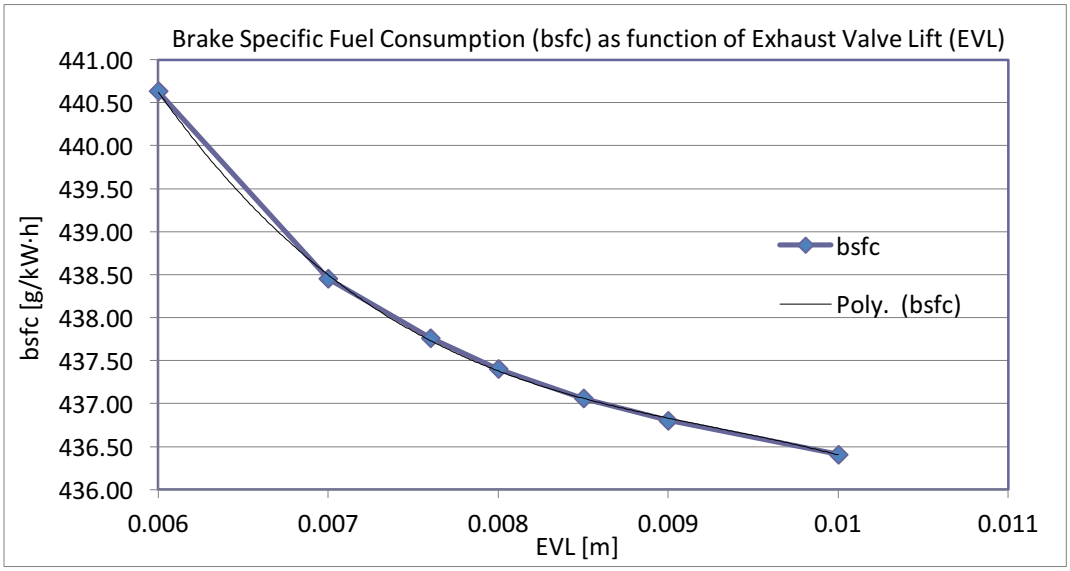

Figure 2.29. Evolution of bsfc with EVL and a constant IVL = 0.00143 m.

From Figure 2.26 to Figure 2.29 it may seem that there is a significant reduction in bsfc. However, by analyzing the data more closely it can be concluded that the reduction in bsfc is not very significant for any of the mentioned graphs. With these results it can be concluded that the decrease in bsfc is not worth the implementation of variable exhaust valve lift technology on the valve train, since it would require a greater production cost that is not compensated by the reduction in bsfc.

3. VALVE TRAIN DESIGN

3.1. Overview

The fresh mixture of air and fuel is conducted to the cylinder (port fuel injection) at the beginning of a new cycle, and the products of combustion are removed at the cycle's end. To do so, engines need to be equipped with devices that are capable of opening and closing the intake and exhaust ports of the cylinder head. The devices that carry out this task are the **intake** and **exhaust valves**. Both types of valves are controlled by the camshaft(s).

"The major function of a camshaft is to open the valves. Camshafts have eccentric shapes called lobes (Figure 3.1) that open the valve against the force of the valve springs. The valve spring closes the valve when the camshaft rotates off of the lobe. The camshaft lobe changes rotary motion (camshaft) to linear motion (valves). Cam shape or contour is the major factor in determining the operating characteristics of the engine. (…) Cam lobe shape has more control over engine performance characteristics than any other single engine part" [13].

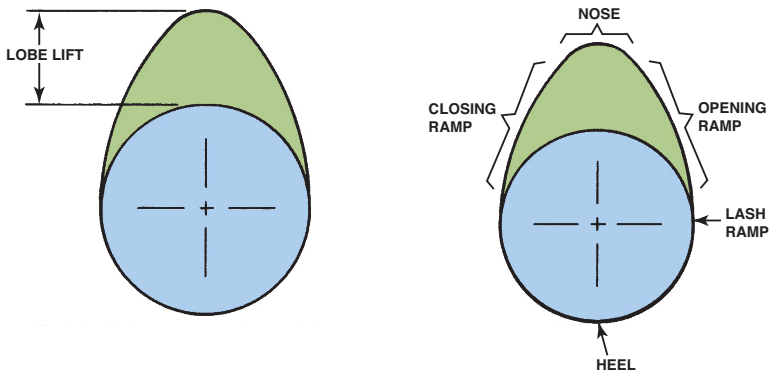

Figure 3.1. Cam lobe [6].

During regular driving, an internal combustion engine is subject to innumerous different situations. It is therefore mandatory for a power unit to have a strong adaptability without losing its reliability. For an engine to be as flexible as possible, it needs to be equipped with **variable valve train systems**, in order to control both valve timing and valve lift.

With a variable valve lift system, the volume of fresh air is regulated by increasing/decreasing the amount of lift of the intake valves. Figure 3.2 and Figure 3.3 show this regulation by presenting the valve lift variation as function of crank angle. With this kind of technology there is no need to use a throttle valve in the vast majority of driving scenarios (some manufacturers choose to include it for safety reasons or to use in a few number of occasions).

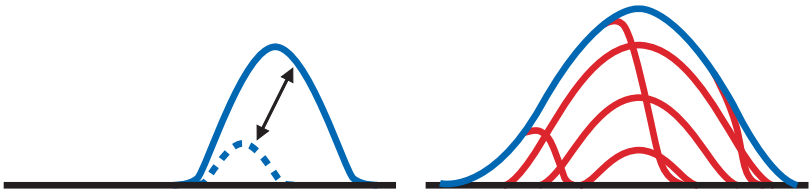

Figure 3.2. Variable valve train with discrete (left) and continuous (right) systems [13].

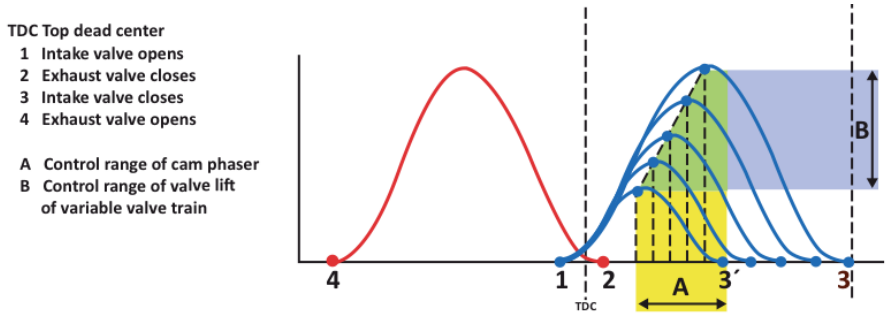

Figure 3.3. Variable valve train effect on engine behavior [13].

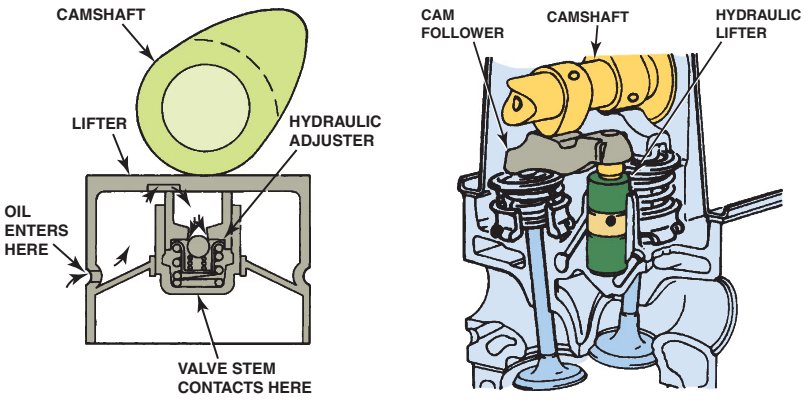

Figure 3.4. Schematic example of a bucket tappet valve actuation mechanism (left) and a finger follower valve actuation mechanism (right) [6].

It is a goal of this dissertation to analyze, select and design the best possible variable valve lift mechanism. For that purpose, two different valve train architectures are analyzed: the **bucket tappet** (Figure 3.4) and the **finger follower** (Figure 3.4) valve trains.

3.2. Bucket Tappet Valve Train

3.2.1. System Considerations

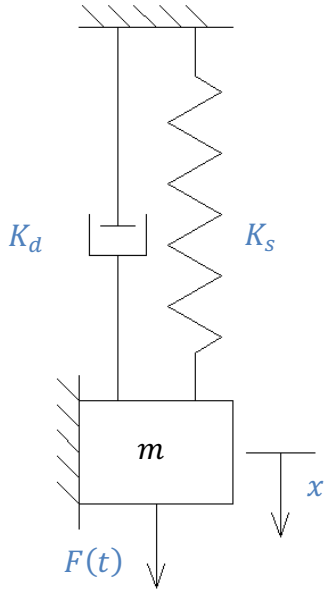

Figure 3.5. Schematic representation of the considered *mass-spring-damper* system.

For the valve train analysis, a *mass-spring-damper* system is used. The system is analyzed for the highest engine speed considered: n = 6000 rpm. As depicted in Figure 3.5, this type of system consists of a mass m that is connected with a spring and a damper. The spring's characteristic feature is the spring rate, K_s, whereas the damper is characterized by the damping coefficient, K_d. Mass m is actuated by a variety of different forces, with $F(t)$ being the resulting one. It actuates on mass m causing a displacement – x. The goal of this analysis is to study the behavior of the **valve train's moving components**. Those components are the masses set in motion by the cam's actuation on the bucket tappet.

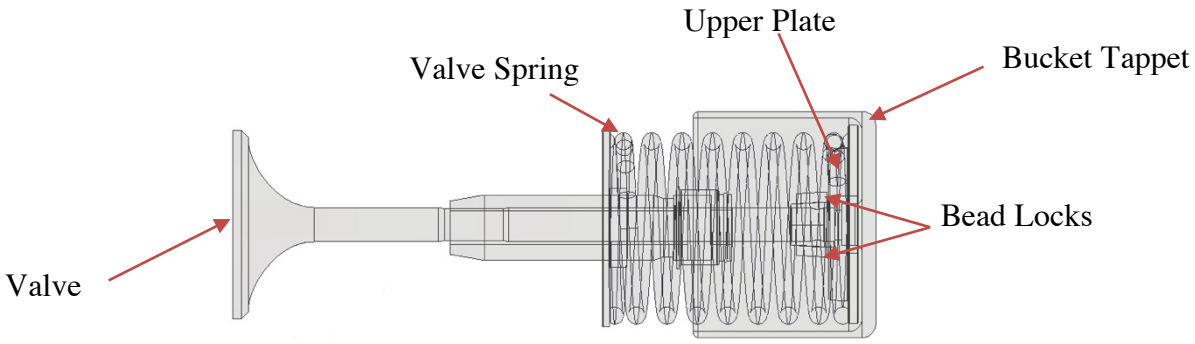

Figure 3.6. Schematic representation of all the system's components. The captioned masses are analyzed as being one mass only.

In this case, mass *m* represents the sum of every moving component that is being analyzed. In order to simplify this analysis, some assumptions are made:

- All of the moving components that are being analyzed are addressed as being one mass only (*m*);
- The previous assumption is valid as long as the spring's force is positive, which in this case means the bucket tappet does not lose contact with the cam;

As depicted in Figure 3.6, the moving components are:

- Valve
- Valve Spring
- Upper Plate
- Valve Spring
- Bead Locks
- Bucket Tappet

Each moving component was designed in Autodesk Inventor 2016 and their mass value is presented on Table 3.1. By summing up the mass of every moving component, the total mass *m* is obtained by Equation (3.1). When the masses of the moving components (valve, valve spring, bead locks, upper plate and bucket tappet) have a given displacement, the spring's center of mass has only one half of that displacement. Because of this, only half of the valve spring's mass is considered.

$$m = m_{\text{valve}} + m_{\text{bead locks}} + m_{\text{upper plate}} + m_{\text{bucket tappet}} + \frac{1}{2} \cdot m_{\text{spring}} \tag{3.1}$$

Table 3.1. Masses of moving components.

Masses of Moving Components	
Intake	
Valve (m_{valve}) [kg]	0.028911
Bead Locks ($m_{\text{bead locks}}$) [kg]	0.000494
Upper Plate ($m_{\text{upper plate}}$) [kg]	0.016269
Bucket Tappet ($m_{\text{bucket tappet}}$) [kg]	0.031445
Valve Spring (m_{spring}) [kg]	0.041790
Total Mass (m) [kg]	0.098014
Exhaust	
Valve (m_{valve}) [kg]	0.026030
Bead Locks ($m_{\text{bead locks}}$) [kg]	0.000494
Upper Plate ($m_{\text{upper plate}}$) [kg]	0.015968
Bucket Tappet ($m_{\text{bucket tappet}}$) [kg]	0.031445
Valve Spring (m_{spring}) [kg]	0.038248
Total Mass (m) [kg]	0.093061

The cam, which is part of the camshaft, rotates in the clockwise direction and actuates directly on the mechanism (Figure 3.7). The mechanism acquires a linear movement downwards (positive direction of x as shown in Figure 3.7) with a displacement x that is equal to the valve lift imposed by the cam.

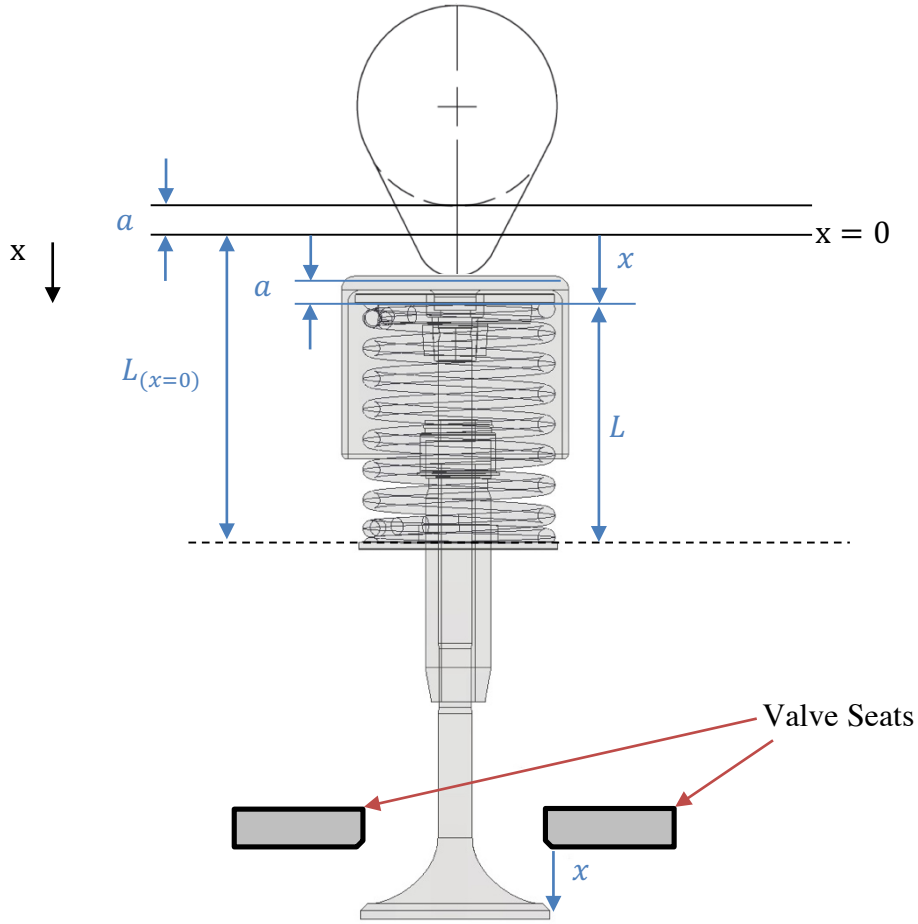

Figure 3.7. Schematic representation of forces and displacements on the valve and its components. The system is actuated directly by the cam on the tappet's top end.

The system can be schematically represented by Figure 3.7. Being:

- x – Valve lift/displacement;
- L_0 – Free length of the valve spring;
- L – Valve spring length for a given x;
- $L_{(x=0)}$ – Valve spring length when $x = 0$/Maximum length of the valve spring after being assembled between the upper and lower valve plates;
- x_0 – Difference in length between L_0 and $L_{(x=0)}$;
- a – Bucket tappet's top thickness;

3.2.2. Length and Displacement Relations

With valve lift and Figure 3.7 it is possible to obtain the valve spring's length at any value of x:

$$x = L_{(x=0)} - L \Leftrightarrow L = L_{(x=0)} - x \tag{3.2}$$

Also, if $x = 0$ (valve closed):

$$L = L_{(x=0)} \tag{3.3}$$

which is the maximum length that can be obtained by the valve spring.

Finally x_0 can be defined as:

$$-x_0 = L_0 - L_{(\mathrm{x=0})} \Leftrightarrow x_0 = L_{(\mathrm{x=0})} - L_0 < 0 \tag{3.4}$$

In this case x_0 is inferior to zero because of the convention made to the positive direction of x.

3.2.3. Spring Rate and Damping Coefficient

As previously stated, both spring and damper have characteristic features - K_s and K_d - respectively. To determine the spring and damping forces it is necessary to define both spring rate and damping constant first. The spring rate is defined once (for the valve spring) [17].

- **Spring Rate**, K_s

$$K_s = \frac{d^4 \cdot G}{8 \cdot D^3 \cdot N_a \cdot \left(1 + \frac{1}{2 \cdot C^2}\right)} \tag{3.5}$$

Being:

d – Spring wire diameter [m];

D – Average spring diameter [m];

N_a – Number of active coils;

G – Torsional modulus of elasticity [Pa]:

$$G = \frac{E}{2 \cdot (1 + \nu)} \tag{3.6}$$

E – Modulus of elasticity [Pa];

ν – Poisson's ratio;

C – Spring index:

$$C = \frac{D}{d} \tag{3.7}$$

The spring rate is calculated using Equations (3.5), (3.6) and (3.7), as well as the information from Table 3.2 and Table 3.3. Both intake and exhaust spring rates are presented in Table 3.4.

Table 3.2. Valve spring dimensions.

Valve Spring Dimensions	
Intake	
Spring Wire Diameter (d) [m]	0.003
Spring Inner Diameter (D_i) [m]	0.023
Average Spring Diameter (D) [m]	0.026
Spring Index (C)	8.667
Number of Active Coils (N_a)	7.75
Exhaust	
Spring Wire Diameter (d) [m]	0.003
Spring Inner Diameter (D_i) [m]	0.0229
Average Spring Diameter (D) [m]	0.0259
Spring Index (C)	8.633
Number of Active Coils (N_a)	7.0

Table 3.3. Spring wire mechanical properties [32].

Spring Wire Mechanical Properties	
Intake	
Torsional Elasticity Modulus (G) [Pa]	8.15×10^{10}
Elasticity Modulus (E) [Pa]	2.06×10^{11}
Poisson's Ratio (v) [m]	0.2638
Exhaust	
Torsional Elasticity Modulus (G) [Pa]	8.15×10^{10}
Elasticity Modulus (E) [Pa]	2.06×10^{11}
Poisson's Ratio (v) [m]	0.2638

Table 3.4. Spring rates.

Spring Rate	
Intake	
Spring Rate (K_s) [N/m]	6017.98
Exhaust	
Spring Rate (K_s) [N/m]	6739.89

The damping coefficient is defined twice: for the valve guide and for the bucket tappet. It is necessary to define two damping coefficients in order to study the friction forces and friction work on both situations:

1. Between the exterior of the valve stem and the interior of the valve guide (Figure 3.8);
2. Between the bucket tappet's exterior and the interior of the bucket tappet guide (Figure 3.8).

There is engine oil between each pair of surfaces.

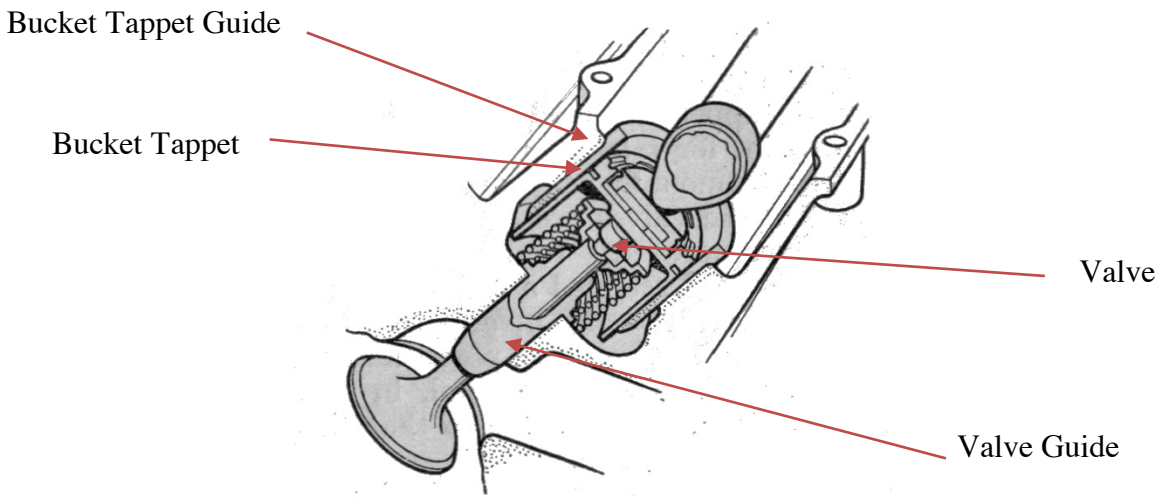

Figure 3.8. Schematic representation of a bucket tappet mechanism mounted on the engine [14].

- **Damping Coefficient**, K_d
  - Valve Guide, K_{dVG}

$$K_{dVG} = \mu(T) \cdot \frac{2 \cdot \pi \cdot D_s \cdot L_{VG}}{(DI_{VG} - D_s)} \quad (3.8)$$

Being:

$\mu(T)$ – Dynamic viscosity of oil (T- Temperature [°C]);

D_s – Valve stem diameter;

L_{VG} – Valve guide length;

DI_{VG} – Valve guide inner diameter;

With Equation (3.8) and the information from Table 3.5, the valve guide's damping coefficient is calculated (Table 3.6).

Table 3.5. Valve and valve guide dimensions.

Valve and Valve Guide Dimensions	
Intake	
Valve Stem Diameter (D_s) [m]	4.985×10^{-3}
Valve Guide Length (L_{VG}) [m]	3.45×10^{-2}
Valve Guide Inner Diameter (DI_{VG}) [m]	5.01×10^{-3}
Valve External Seat Diameter (D_{vi}) [m]	0.0275
Valve Seat Width (w) [m]	0.001
Valve Seat Angle (β) [°]	45
Exhaust	
Valve Stem Diameter (D_s) [m]	4.98×10^{-3}
Valve Guide Length (L_{VG}) [m]	3.45×10^{-2}
Valve Guide Inner Diameter (DI_{VG}) [m]	5.01×10^{-3}
Valve External Seat Diameter (D_{ve}) [m]	0.0236
Valve Seat Width (w) [m]	0.00096
Valve Seat Angle (β) [°]	45

Table 3.6. Valve guide damping coefficient.

Damping Coefficient – Valve Guide	
Intake	
Damping Coefficient (K_{dVG}) [N·s/m]	0.35
Exhaust	
Damping Coefficient (K_{dVG}) [N·s/m]	0.29

- Bucket Tappet, K_{dBT}

$$K_{\mathrm{dBT}} = \mu(T) \cdot \frac{2 \cdot \pi \cdot DE_{\mathrm{BT}} \cdot L_{\mathrm{BT}}}{\left(DI_{\mathrm{BTG}} - DE_{\mathrm{BT}}\right)} \tag{3.9}$$

Being:

$\mu(T) = 8.098\times10^{-3}$ Pa · s – Dynamic viscosity of oil;

DE_{BT} – Bucket tappet outer diameter;

L_{BT} – Bucket tappet length;

DI_{BTG} – Bucket tappet guide inner diameter;

With Equation (3.9) and the information from Table 3.7, the bucket tappet's damping coefficient is calculated (Table 3.8).

Table 3.7. Bucket tappet dimensions.

Bucket Tappet Dimensions	
Intake	
Bucket Tappet Outer Diameter (DE_{BT}) [m]	0.032
Bucket Tappet Length (L_{BT}) [m]	0.0239
Bucket Tappet Guide Inner Diameter (DI_{BTG}) [m]	0.032025
Exhaust	
Bucket Tappet Outer Diameter (DE_{BT}) [m]	0.032
Bucket Tappet Length (L_{BT}) [m]	0.0239
Bucket Tappet Guide Inner Diameter (DI_{BTG}) [m]	0.032025

Table 3.8. Bucket tappet damping coefficient.

Damping Coefficient – Bucket Tappet	
Intake	
Damping Coefficient (K_{dBT}) [N·s/m]	1.56
Exhaust	
Damping Coefficient (K_{dBT}) [N·s/m]	1.56

3.2.4. Forces

- **Spring Force**, F_{spring}

Spring force is the force exerted by the spring on the moving masses of the system. For a system with a linear behavior, the spring force (F_{spring}) is given by Equation (3.10) [15].

$$F = K \cdot x \tag{3.10}$$

With F being F_{spring}, K the spring rate (K_s), and x the displacement as previously defined. With Equation (3.10) and the previously defined length and displacement relations comes Equation (3.11).

$$\begin{aligned} F_{\mathrm{spring}} &= K_s \cdot (L - L_0) = -K_s \cdot (L_0 - L) = -K_s \cdot \left(L_0 - L_{(x=0)} + x\right) \\ &= -K_s \cdot (x - x_0) \end{aligned} \tag{3.11}$$

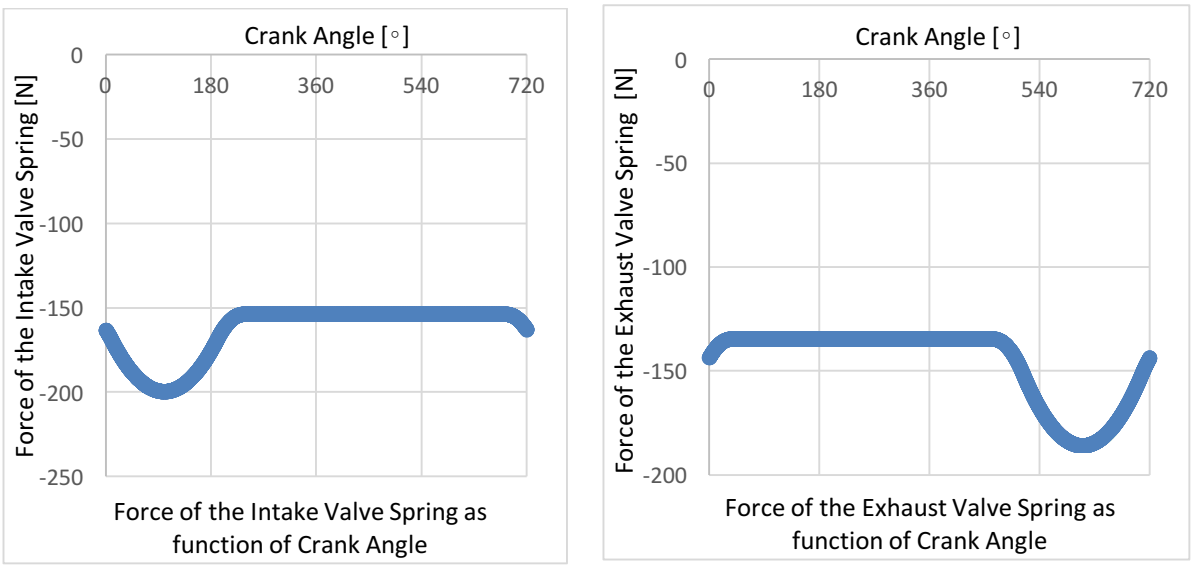

Figure 3.9. Force of the intake (left) and the exhaust (right) valve spring as function of crank angle.

The force of the intake and the exhaust valve spring throughout the engine cycle is depicted on Figure 3.9 (left and right respectively). On the intake valve spring, the minimum and maximum forces (in module) are, respectively, 154 N and 200 N. The exhaust valve spring's minimum and maximum forces (in module) are, respectively, 135 N and 186 N. The minimum forces in the valve springs are registered when the valves are closed. When the force of the valve springs starts to increase, it means that the valves are opening.

- **Damping Force**, F_{damping}

Damping force (F_{damping}) is given by Equation (3.12).

$$F = -K \cdot \frac{dx}{dt} \tag{3.12}$$

With F being F_{damping}, K the sum of both damping coefficients (K_d), and x the displacement as previously defined.

$$F_{\text{damping}} = -(K_{\text{dVG}} + K_{\text{dBT}}) \cdot \frac{dx}{dt} \tag{3.13}$$

- **Weight Force**, F_{weight}

Weight force (F_{weight}) is given by Equation (3.14).

$$F = m \cdot g \tag{3.14}$$

Being:

$g = 9.81\ \text{m/s}^2$ – Gravitational acceleration;

- **Pressure Force**, F_{pressure}

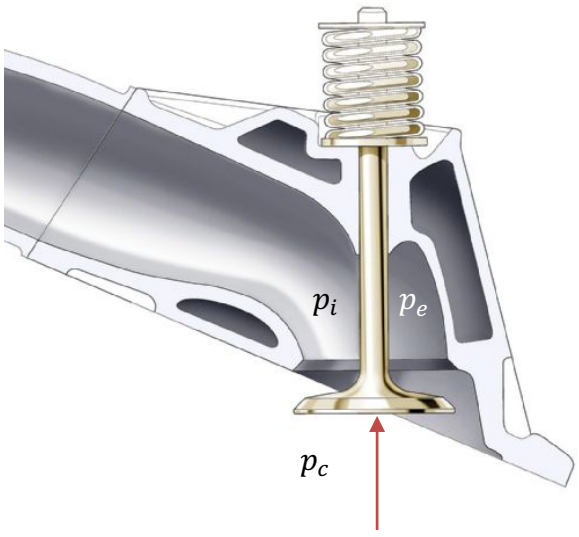

Figure 3.10. Schematic representation of the pressure inside the cylinder and on the inlet/outlet port [16].

Figure 3.10 depicts a schematic representation of the pressure inside the cylinder (p_c) and on the inlet (p_i)/outlet (p_e) port. Pressure force, F_{pressure}, can be defined as the force created by the pressure difference between the engine's cylinder and the inlet/outlet port. To simplify this subchapter's following equations, F_{pressure} will be referred to as:

F_{pe} – Pressure force on the exhaust valves;

F_{pi} – Pressure force on the intake valves;

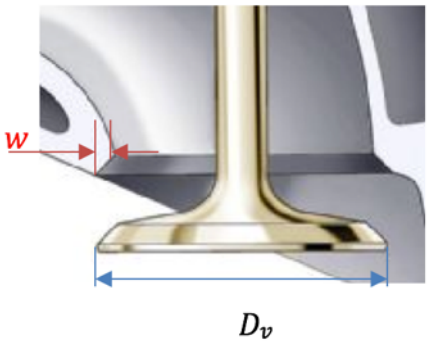

Figure 3.11. Schematic figure showing the width of the valve seat and the external seat diameter of the valve [16].

- Exhaust

$$F_{\text{pe}} = p_e \cdot \frac{\pi}{4} \cdot (D_{\text{ie}}^2 - D_{\text{se}}^2) + p_{\text{atm}} \cdot \frac{\pi}{4} \cdot D_{\text{se}}^2 + \frac{(p_e + p_c)}{2} \cdot \frac{\pi}{4} (D_{\text{ve}}^2 - D_{\text{ie}}^2) - p_c \cdot \frac{\pi}{4} \cdot D_{\text{ve}}^2 \quad (3.15)$$

$$\leftrightarrow F_{\text{pe}} = \frac{\pi}{4} \cdot \left[p_e \cdot (D_{\text{ie}}^2 - D_{\text{se}}^2) + p_{\text{atm}} \cdot D_{\text{se}}^2 + \frac{(p_e + p_c)}{2} \cdot (D_{\text{ve}}^2 - D_{\text{ie}}^2) - p_c \cdot D_{\text{ve}}^2 \right]$$

With:

$$D_{\text{ie}} = D_{\text{ve}} - 2 \cdot w \quad (3.16)$$

Being:

D_{ie} – Exhaust valve inner seat diameter;

D_{se} – Exhaust valve stem diameter;

D_{ve} – Exhaust valve external seat diameter;

p_{atm} – Atmospheric pressure;

w – Valve seat width (Figure 3.11)

- Intake

$$F_{\text{pi}} = \frac{\pi}{4} \cdot \left[p_i \cdot (D_{\text{ii}}^2 - D_{\text{si}}^2) + p_{\text{atm}} \cdot D_{\text{si}}^2 + \frac{(p_i + p_c)}{2} \cdot (D_{\text{vi}}^2 - D_{\text{ii}}^2) - p_c \cdot D_{\text{vi}}^2 \right] \quad (3.17)$$

Being:

D_{ii} – Intake valve inner seat diameter;

D_{si} – Intake valve stem diameter;

D_{vi} – Intake valve external seat diameter;

- **Valve Seat Force**, F_{seat}

The valve seat force is the force exerted by the valve seat when in contact with the valve. To define the valve seat force, it is necessary to apply Newton's second law of motion to the system:

$$\Sigma F = m \cdot a$$
$$\Leftrightarrow F_{pressure} + F_{spring} + F_{damping} + F_{weight} + F_{seat} + F_{cam} = m \cdot \frac{d^2x}{dt^2} \quad (3.18)$$

On one hand, if $x = 0$, then:

$$\Rightarrow \frac{d^2x}{dt^2} = 0;\ \frac{dx}{dt} = 0;\ F_{cam} = 0$$

On $x = 0$ there is no force being applied by the cam on the tappet and both acceleration and velocity are null because the system has no motion. The valve seat force balances all the other forces. Equation (3.18) becomes:

$$F_{seat} = -m \cdot g + K_s(0 - x_0) - F_{pressure} \quad (3.19)$$

which is the equation for the force applied by the valve seat on mass m. Figure 3.12 shows the force of the intake and exhaust valve seats (left and right, respectively) during an engine cycle.

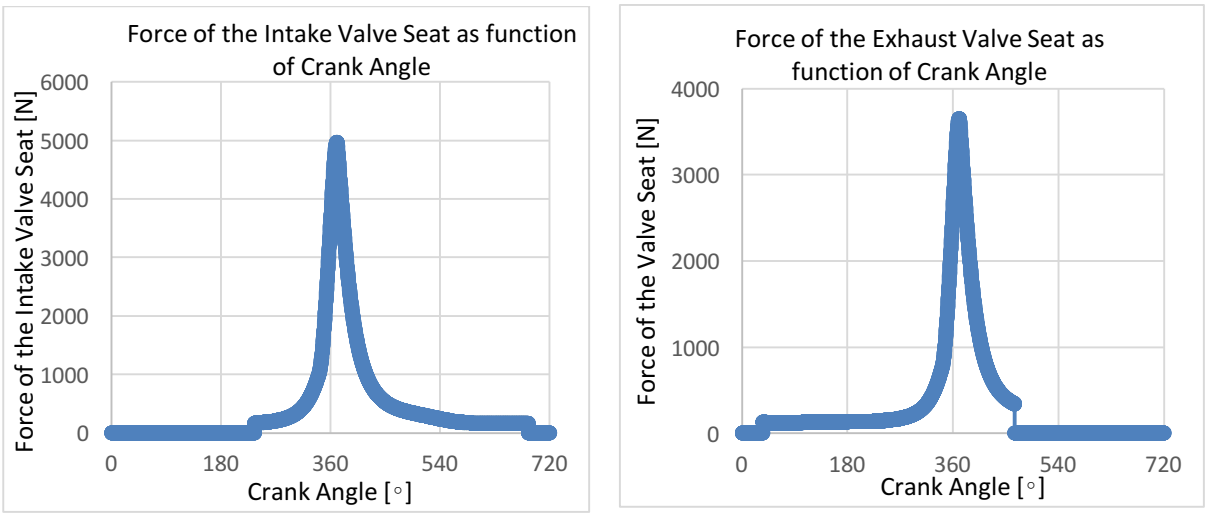

Figure 3.12. Force of the intake (left) and exhaust (right) valve seat as function of crank angle.

- **Cam Force**, F_{cam}

The cam force is the force exerted by the cam when in contact with the bucket tappet. Using (3.18) and $x > 0$, then:

$$\Rightarrow F_{\text{seat}} = 0$$

Mass m is no longer in contact with the valve seat. It is being actuated by the cam. Equation (3.18) becomes:

$$-K_s(x - x_0) - K_d \cdot \frac{dx}{dt} + m \cdot g + F_{\text{cam}} + F_{\text{pressure}} = m \cdot \frac{d^2x}{dt^2} \quad (3.20)$$

$$\Leftrightarrow F_{\text{cam}} = K_s \cdot (x - x_0) + K_d \cdot \frac{dx}{dt} - m \cdot g + m \cdot \frac{d^2x}{dt^2} - F_{\text{pressure}}$$

which is the force applied by the cam on the bucket tappet's top end.

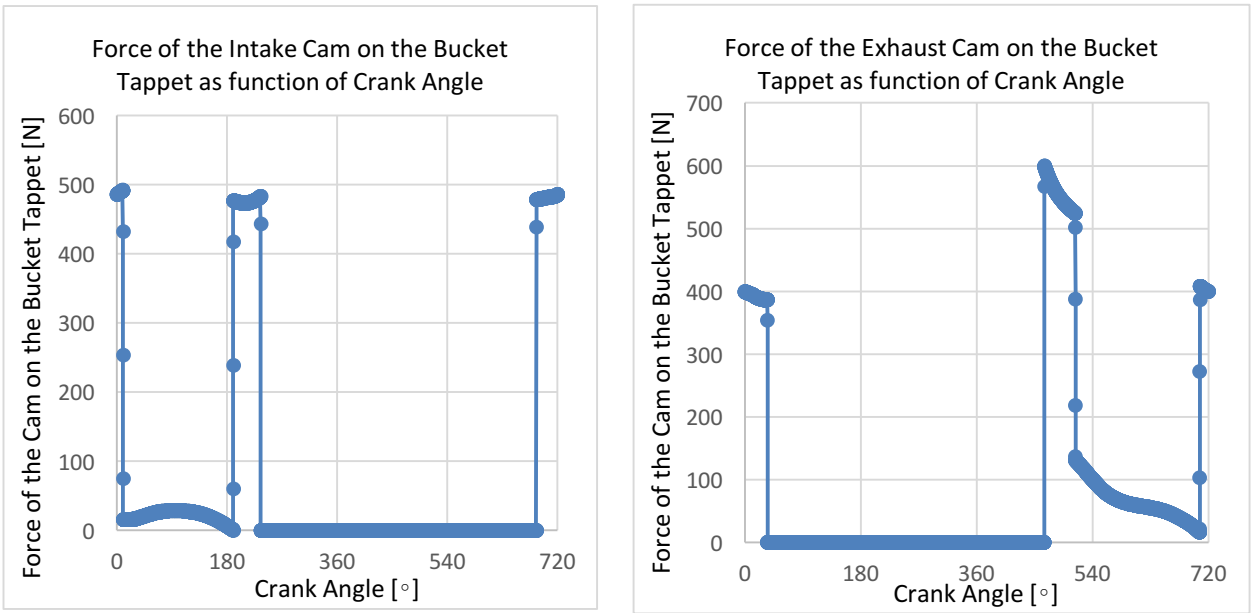

Figure 3.13. Force applied by the intake (left) and exhaust (right) cam on the tappet's top end as function of crank angle.

One of the most sensible aspects of valve train design, is to ensure that the cam and the bucket tappet do not lose contact. This aspect is obviously deeply related to the valve spring of the mechanism, which is responsible for maintaining the cam and bucket tappet in contact with each other. On Figure 3.13 the forces of the intake and exhaust cam (left and right, respectively) never acquire a negative value, which would, in that case, mean that the contact between the cam and the bucket tappet had been lost. Figure 3.13 shows that the force exerted by the exhaust cam on the bucket tappet reaches higher maximum values than

the force exerted by the intake cam on the bucket tappet. This is due to the high pressure inside the cylinder at the time the exhaust valve is opened.

- **Friction Forces**, F_{friction}
  - Valve Guide

The friction force between the valve stem's exterior and the valve guide's interior is given by Equation (3.21). Figure 3.14 and Figure 3.15 schematically represent the valve guide and the valve stem.

$$\begin{aligned} F_{\text{frictionVG}} &= -\tau \cdot A = -\mu \cdot \frac{dV}{dy} \cdot \pi \cdot D_s \cdot L_{\text{VG}} \\ &= -\mu \cdot \frac{dx}{dt} \cdot \frac{2}{\left(DI_{\text{VG}} - D_s\right)} \cdot \pi \cdot D_s \cdot L_{\text{VG}} \\ &= -\mu(T) \cdot \frac{2 \cdot \pi \cdot D_s \cdot L_{\text{VG}}}{(DI_{\text{VG}} - D_s)} \cdot \frac{dx}{dt} \end{aligned} \tag{3.21}$$

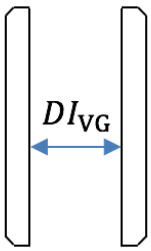

Figure 3.14. Schematic representation of the valve guide's inner diameter.

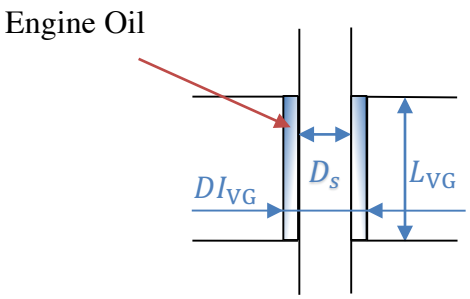

Figure 3.15. Schematic representation of the valve stem, the valve guide, and the engine oil between them.

- Bucket Tappet

The friction force between the bucket tappet and the bucket tappet's interior is given by Equation (3.22).

$$\begin{aligned} F_{\text{frictionBT}} &= -\tau \cdot A = -\mu \cdot \frac{dV}{dy} \cdot \pi \cdot DE_{\text{BT}} \cdot L_{\text{BT}} \\ &= -\mu \cdot \frac{dx}{dt} \cdot \frac{2}{(DI_{\text{BTG}} - DE_{\text{BT}})} \cdot \pi \cdot DE_{\text{BT}} \cdot L_{\text{BT}} \\ &= -\mu(T) \cdot \frac{2 \cdot \pi \cdot DE_{\text{BT}} \cdot L_{\text{BT}}}{(DI_{\text{BTG}} - DE_{\text{BT}})} \cdot \frac{dx}{dt} \end{aligned} \tag{3.22}$$

3.2.5. Friction Work

Having defined the friction forces, it is now possible to evaluate the friction work. The intake bucket tappet friction work is presented on Figure 3.16.

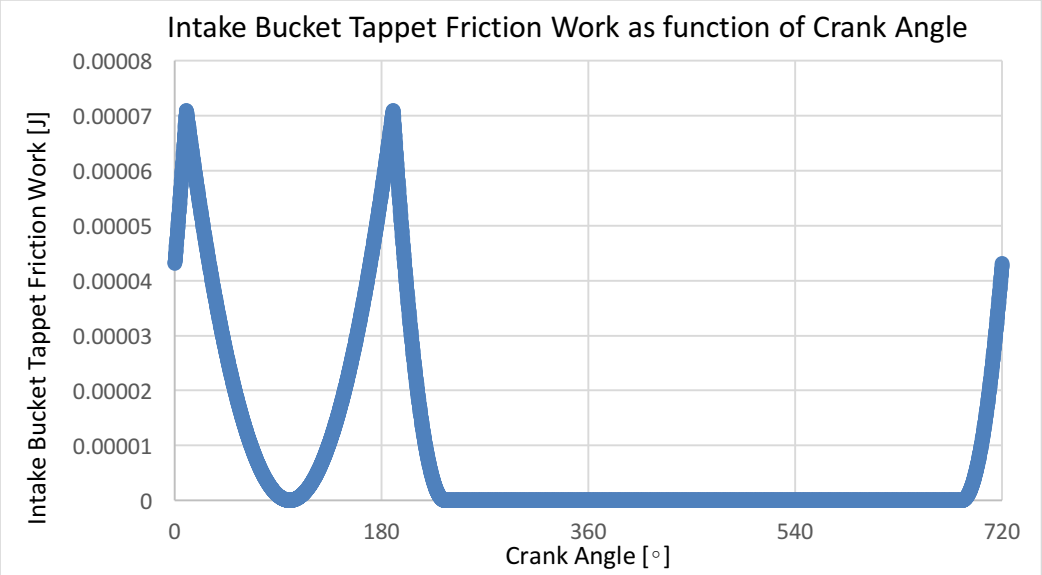

Figure 3.16. Intake bucket tappet friction work as function of crank angle.

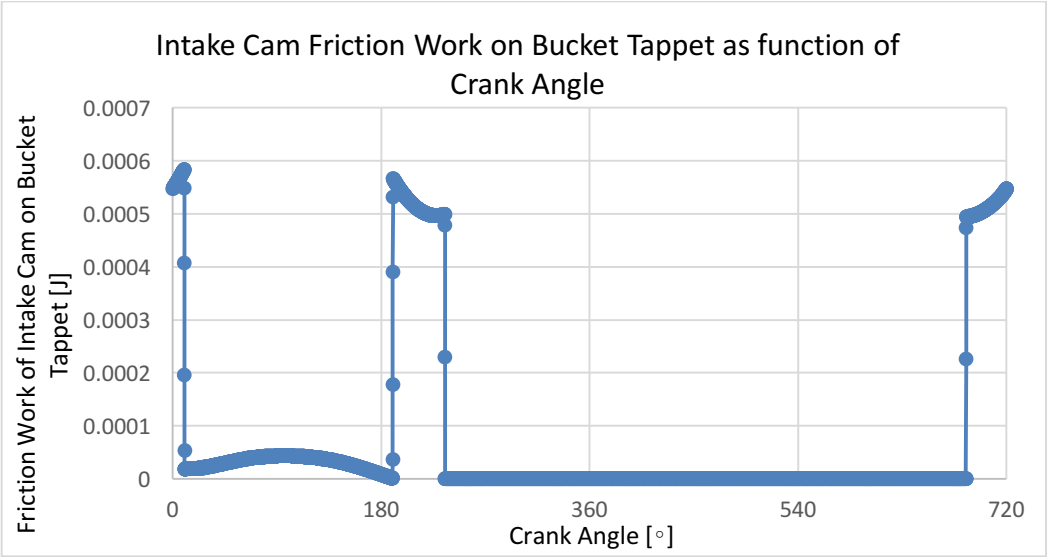

Figure 3.17. Intake cam friction work on bucket tappet as function of crank angle.

The friction work of the intake cam on the bucket tappet is also shown on Figure 3.17, whereas Figure 3.18 presents the intake valve guide friction work. The evolution of the intake cam friction work on the bucket tappet throughout the cycle (Figure 3.17) is very similar to the behavior of the intake cam force on the bucket tappet (left side of Figure 3.13). On both Figure 3.16 and Figure 3.18, the highest values of friction work are obtained at the opening and closing of the intake valves.

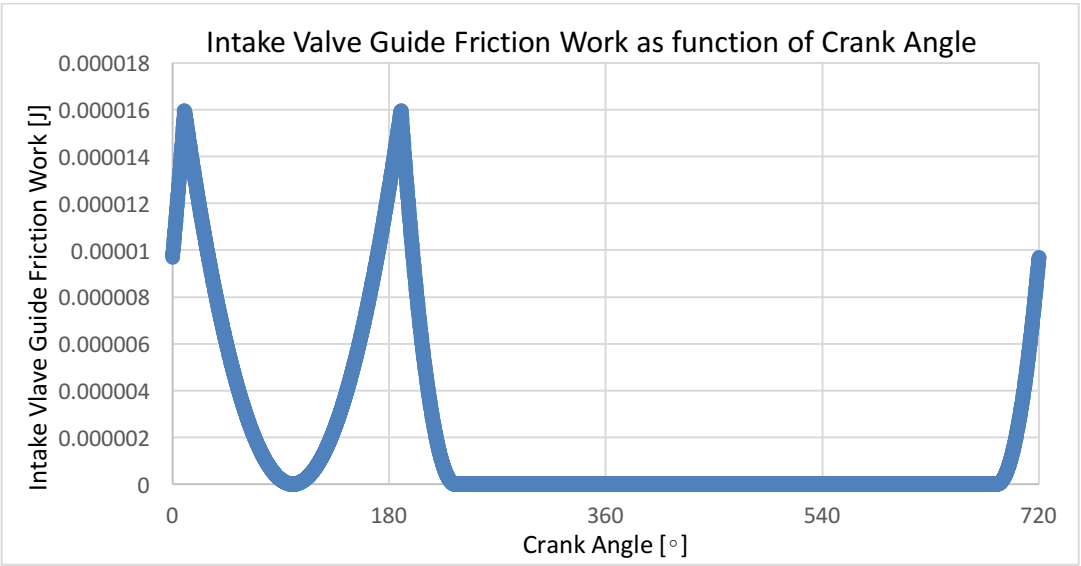

Figure 3.18. Intake valve guide friction work as function of crank angle.

The exhaust bucket tappet friction work is presented on Figure 3.19.

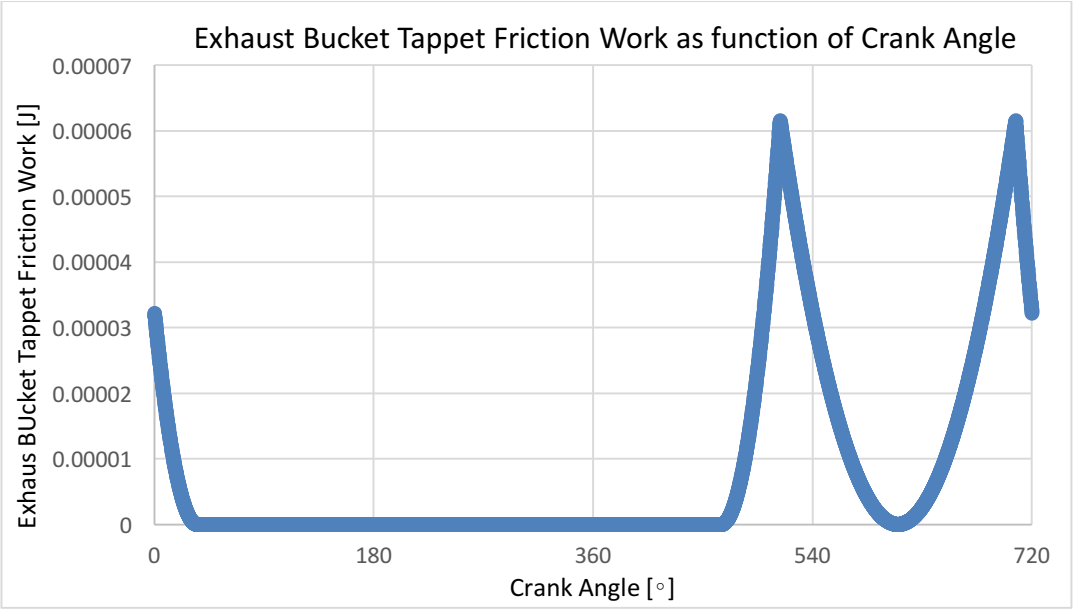

Figure 3.19. Exhaust bucket tappet friction work as function of crank angle.

The friction work of the exhaust cam on the bucket tappet is also shown on Figure 3.20, whereas Figure 3.21 presents the exhaust valve guide friction work. The evolution of the exhaust cam friction work on the bucket tappet throughout the cycle (Figure 3.20) is very similar to the behavior of the exhaust cam force on the bucket tappet (right side of Figure 3.13). On both Figure 3.19 and Figure 3.21, the highest values of friction work are obtained at the opening and closing of the exhaust valves.

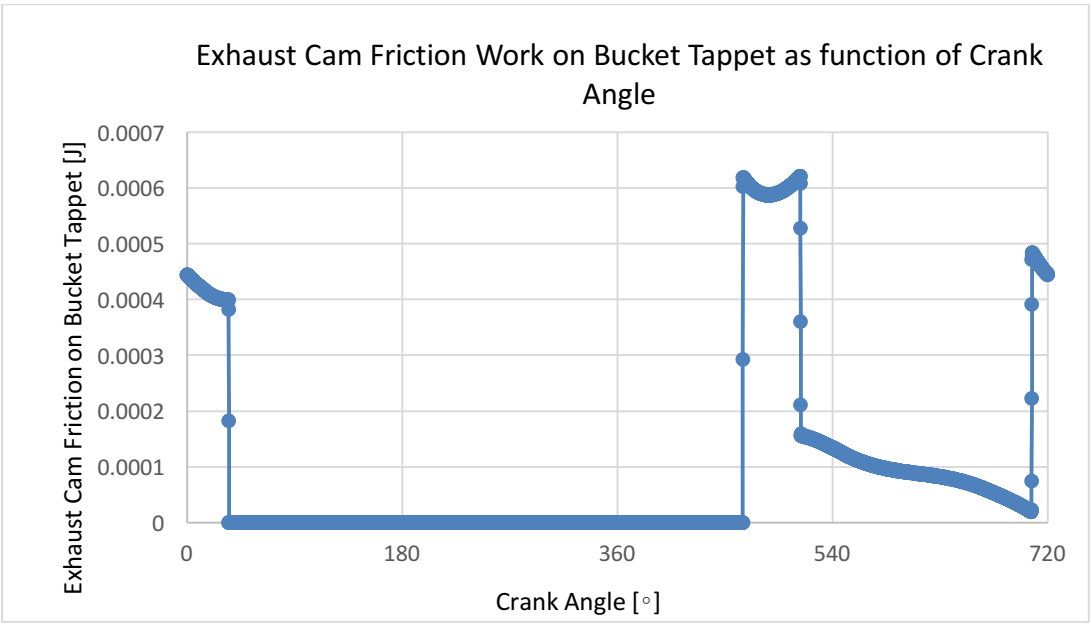

Figure 3.20. Exhaust cam friction work on bucket tappet as function of crank angle.

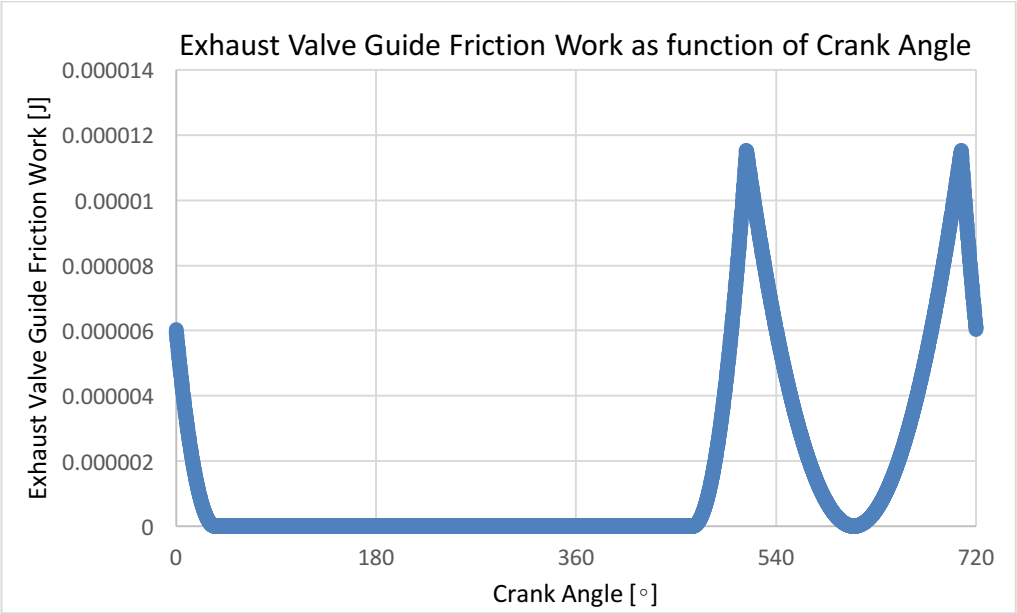

Figure 3.21. Exhaust valve guide friction work as function of crank angle.

3.2.6. Type of Spring Ends

The type of spring ends used has direct influence on the spring's behavior. In this case, both intake and exhaust valve springs have a squared and grounded end on both sides.

3.2.7. Stability

According to [17], compression coil springs may buckle when the deflection becomes too large. The critical deflection is given by Equation (3.23):

$$y_{cr} = L_0 \cdot C_1' \left[1 - \left(1 - \frac{C_2'}{\lambda_{eff}^2}\right)^{1/2}\right] \tag{3.23}$$

Being:

y_{cr} – Critical Deflection (corresponding to the onset of instability)

C_1' – Elastic constant:

$$C_1' = \frac{E}{2 \cdot (E - G)} \tag{3.24}$$

C_2' – Elastic constant:

$$C_2' = \frac{2 \cdot \pi^2 \cdot (E - G)}{2 \cdot G + E} \tag{3.25}$$

λ_{eff} – Effective slenderness ratio:

$$\lambda_{eff} = \frac{\alpha \cdot L_0}{D} \tag{3.26}$$

Being:

$\boldsymbol{\alpha}$ – End-condition constant (as shown in Table 3.9, $\boldsymbol{\alpha = 0.5}$)

Table 3.9. Valve spring's end condition.

End Condition for helical compression springs	End-Condition Constant α for both Intake and Exhaust Valve Springs
Spring supported between flat parallel surfaces (fixed ends)	0.5

Table 3.10. Valve spring's stability.

Stability	
Intake	
Critical Deflection (y_{cr}) [m]	0.111
Elastic Constant (C_1')	0.827
Elastic Constant (C_2')	6.66
Effective Slenderness Ratio (λ_{eff})	1.285
Exhaust	
Critical Deflection (y_{cr}) [m]	0.111
Elastic Constant (C_1')	0.827
Elastic Constant (C_2')	6.66
Effective Slenderness Ratio (λ_{eff})	1.178

There is absolute stability when:

$$\frac{C_2'}{\lambda_{eff}^2} > 1 \tag{3.27}$$

This means that:

$$L_0 < \frac{\pi \cdot D}{\alpha}\left[\frac{2 \cdot (E - G)}{2 \cdot G + E}\right]^{1/2} \tag{3.28}$$

For steel springs, Equation (3.28) becomes Equation (3.29).

$$L_0 < 2.63 \cdot \frac{D}{\alpha} \tag{3.29}$$

With $\alpha = 0.5$:

$$L_0 < 5.26 \cdot D \tag{3.30}$$

Equation (3.30) is therefore the absolute stability condition for this specific case. Table 3.10 and Table 3.11 summarize the valve spring's stability and stability verification. Besides all the previously analyzed factors, it is also necessary to verify that the turns from the valve springs do not touch when operating. To prevent spring turns from touching, valve springs must have a length with a minimum value that is 1.15 times the spring's solid length.

Table 3.11. Absolute valve spring stability verification.

Absolute Stability Verification	
Intake	
$\frac{C_2'}{\lambda_{eff}^2} > 1$	4.036
Maximum Value of L_0 [m]	0.134
Exhaust	
$\frac{C_2'}{\lambda_{eff}^2} > 1$	4.803
Maximum Value of L_0 [m]	0.134

3.2.8. Critical Frequency of Helical Springs

If the spring ends are always in contact with the plates, then the fundamental frequency is given by (3.31) [17]:

$$f\ [\text{Hz}] = \frac{1}{2} \cdot \sqrt{\frac{k \cdot g}{W}} = \frac{1}{2} \cdot \sqrt{\frac{k \cdot g}{m \cdot g}} = \frac{1}{2} \cdot \sqrt{\frac{k}{m}} \tag{3.31}$$

If the frequency is not high enough, the spring should be redesigned to increase k or decrease W. In this case, k is the valve spring rate, K_s, and m is the active coils mass, m_{ac}. To analyze the frequency of the springs, it is necessary to define the period (T) first.

$$T = \frac{\Delta\theta_{\text{valve}}\ [°]}{360°} \cdot \frac{1}{N\ [\text{rot/s}]} \tag{3.32}$$

$$f = \frac{1}{T} \tag{3.33}$$

Table 3.12. Critical frequency of helical springs.

Critical Frequency of Helical Springs	
Intake	
Active Coils Mass (m_{ac}) [kg]	0.035
Fundamental Frequency (f_{fund}) [Hz]	2.07×10^{2}
Period (T) [s]	7.50×10^{-3}
Frequency (f) [Hz]	1.33×10^{2}
(f_{fund}) [Hz] / (f) [Hz]	1.55
Exhaust	
Active Coils Mass [kg]	0.032
Fundamental Frequency (f_{fund}) [Hz]	2.31×10^{2}
Period (T) [s]	8.06×10^{-3}
Frequency (f) [Hz]	1.24×10^{2}
(f_{nat}) [Hz] / (f) [Hz]	1.86

Table 3.12 shows that the fundamental frequency is 1.55 and 1.86 times higher than the spring's frequency, for both intake and exhaust valves, respectively. With this design, the springs don't resonate.

3.2.9. Fatigue Loading of Helical Compression Springs

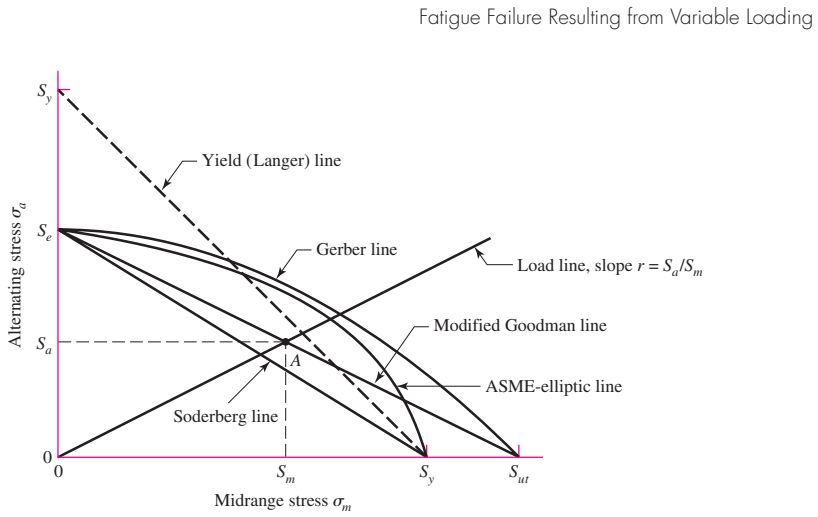

Figure 3.22. Fatigue diagram containing various criteria of failure [17].

Using the Modified Goodman Criterion [17]:

$$\frac{S_a}{S_e} + \frac{S_m}{S_{\text{ut}}} = 1 \leftrightarrow \frac{S_a}{S_e} = 1 - \frac{S_m}{S_{\text{ut}}} \leftrightarrow S_e = \frac{S_a}{1 - \frac{S_m}{S_{\text{ut}}}} \tag{3.34}$$

$$\frac{S_{\text{sa}}}{S_{\text{se}}} + \frac{S_{\text{sm}}}{S_{\text{su}}} = 1 \leftrightarrow \frac{S_{\text{sa}}}{S_{\text{se}}} = 1 - \frac{S_{\text{sm}}}{S_{\text{su}}} \leftrightarrow S_{\text{se}} = \frac{S_{\text{sa}}}{1 - \frac{S_{\text{sm}}}{S_{\text{su}}}} \tag{3.35}$$

Being:

S_a – Alternate strength;

S_e – Endurance strength;

S_m – Average strength;

S_{ut} - Ultimate strength;

S_{se} – Endurance shear strength;

S_{sa} – Alternate shear strength;

S_{su} – Ultimate shear strength;

S_{sm} – Average shear strength

For unpeened steel spring wire:

$$S_{\text{sa}} = 241 \text{ MPa} \tag{3.36}$$

$$S_{\text{sm}} = 379 \text{ MPa} \tag{3.37}$$

$$A = 2211 \text{ MPa} \tag{3.38}$$

$$m_{\text{Goodman}} = 0.145 \tag{3.39}$$

$$S_{\text{ut}} = \frac{2211}{3.0^{0.145}} = 1885 \text{ MPa} \tag{3.40}$$

$$S_{\text{su}} = 0.577 \cdot S_{\text{ut}} = 0.577 \cdot 1885 = 1088 \text{ MPa} \tag{3.41}$$

For unpeened steel spring wire:

$$S_{\text{se}} = \frac{241}{1 - \frac{379}{1088}} = 370 \text{ MPa} \tag{3.42}$$

Using the Modified Goodman Criterion, the safety fatigue factor is given by Equation (3.43).

$$n_f = \frac{1}{\frac{\sigma_a}{S_e} + \frac{\sigma_m}{S_{\text{ut}}}} \tag{3.43}$$

- Intake

$$n_f = \frac{1}{\frac{\tau_a}{S_{\text{se}}} + \frac{\tau_m}{S_{\text{su}}}} = \frac{1}{\frac{65.5}{370} + \frac{507.1}{1088}} = 1.555 \tag{3.44}$$

- Exhaust

$$n_f = \frac{1}{\frac{\tau_a}{S_{\text{se}}} + \frac{\tau_m}{S_{\text{su}}}} = \frac{1}{\frac{73.2}{370} + \frac{458.2}{1088}} = 1.615 \tag{3.45}$$

Being:

A – Ultimate strength of the spring wire for a wire diameter of 1 mm;

m_{sw} – Exponent of the wire diameter for ultimate strength of spring wire;

S_{ut} – Ultimate strength;

n_f – Fatigue safety factor;

σ_a – Alternate stress;

σ_m – Average stress;

τ_a – Alternate shear stress:

$$\tau_a = (\tau_{1\max} - \tau_{1\min})/2 \tag{3.46}$$

τ_1 – Shear stress amplitude:

$$\tau_1 = \left(-K_w \cdot \frac{8 \cdot F_{\text{spring}} \cdot D}{\pi \cdot d^3}\right) \tag{3.47}$$

τ_m – Average shear stress:

$$\tau_m = (\tau_{1\max} + \tau_{1\min})/2$$

With $\tau_{1\max}$ and $\tau_{1\min}$ being the maximum and minimum value (respectively) of the shear stress amplitude (τ_1).

These safety fatigue factors confirm that the springs are well designed. The CAD design of this mechanism is in **Annex B**.

3.3. Finger Follower Valve Train

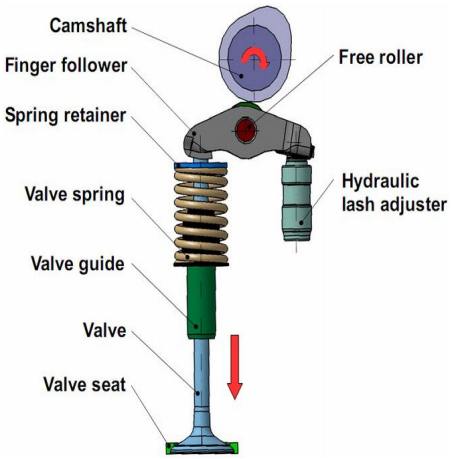

Figure 3.23. Schematic example of a finger follower valve train [18].

The second valve actuation mechanism to be analyzed at n = 6000 rpm was the finger follower valve train. As in the bucket tappet mechanism, this valve train was analyzed with one valve spring per valve only. However, unlike in the previous mechanism, the obtained results were not satisfactory (Figure 3.24). Even after an extensive shape optimization process, the valve spring did not comply with all of the established design criteria. Even with a safety fatigue factor of only 1.2, the cam continues to lose contact with

the mechanism (Figure 3.24). This mechanism is intended for a variable valve train. The analysis, selection and CAD design of this mechanism are presented in **Annex C**.

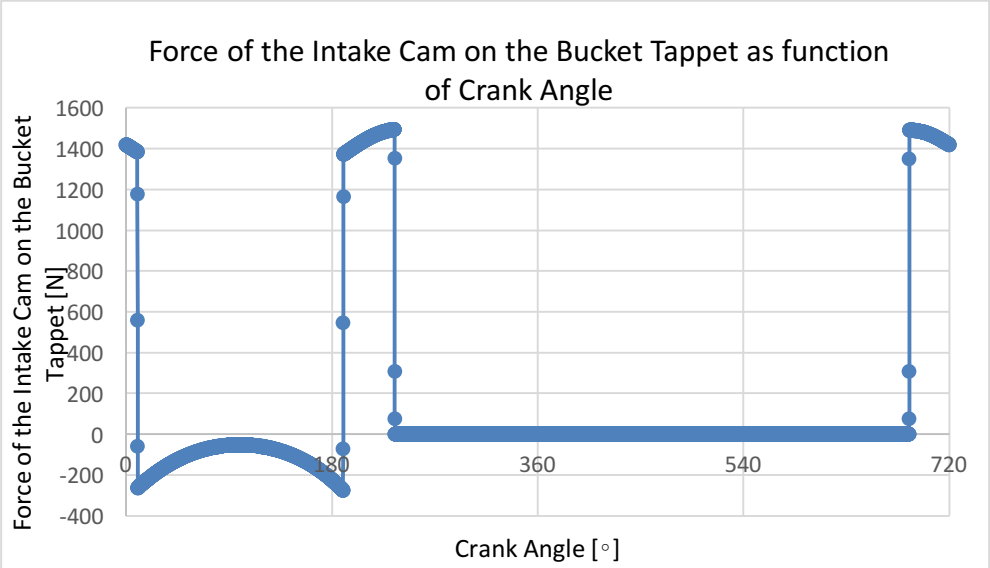

Figure 3.24. Force of the intake cam on the bucket tappet as function of crank angle.

4. CONCLUSIONS

From the introductory chapter there are several conclusions regarding the engine's characteristics. Those characteristics are:

- Type: Four-Stroke;
- Ignition: Spark Ignition;
- Cylinders: Inline Three Cylinder;
- Displacement: 998 cm^3;
- Air Induction: Atmospheric;
- Fuel Injection: Port Fuel Injection;
- Bore: 71.0 mm;
- Stroke: 84.0 mm;
- Stroke/Bore: 1.183;
- Compression Ratio: 11.0:1;
- Valves: 12 Valves – 4 Valves Per Cylinder;
- Valve Train: DOHC – Double Overhead Camshaft;

In chapter 2, two different strategies were used in order to obtain the highest possible brake power and the lowest possible brake specific fuel consumption. It was concluded that the highest **brake power criterion** provides the best results. It was also concluded that the use of a valve train equipped with **variable intake valve lift**, instead of a butterfly throttle valve, leads to a **10% reduction in bsfc**. However, for a valve train equipped with variable exhaust valve lift, the bsfc reduction was not significant. Therefore, variable valve lift should be applied to the intake valves but not to the exhaust valves.

From chapter 3, two mechanisms were analyzed: the bucket tappet valve train and the finger follower valve train. Regarding the **bucket tappet valve train**, the mechanism was successfully designed with one spring (per valve) only. The same result was not obtained for the **finger follower valve train** system (with the same engine speed – n = 6000 rpm). With one spring (per valve) only, the cam did not maintain contact with the mechanism. It may be possible to design this system with two valve springs per valve. This designed is proposed for future work.

Finally, in chapter 4 it is concluded that, out of all of the analyzed systems, **Toyota's Valvematic** is the more advantageous continuous variable valve lift system for this engine.

Future Work Proposals

- Following the conclusions from chapter 3, the finger follower valve train design with two springs per valve is suggested as future work proposal;
- As a continuation to this specific work it is suggested that the camshafts are designed and that the Valvematic valve train's detailed project is continued;
- It is suggested that the engine's detailed project is continued;

BIBLIOGRAPHY

[1] Carvalheira, Pedro. *A Thermodynamic Cycle Model of Four-Stroke Spark Ignition Internal Combustion Engine*. Symposium for Combustion Control, Aachen, 2016.

[2] https://autoandrive.com/2010/05/12/alba-1952-1954/
(Accessed 17/06/2016)

[3] http://ec.europa.eu/clima/policies/transport/vehicles/cars/index_en.html
(Accessed 28/06/2016)

[4] The international council on clean transportation. *CO2 emissions from new passenger cars in the EU: Car manufacturers' performance in 2014*.July 2015

[5] Pita, Hernâni. *Projecto de Um Motor de Combustão Interna para Um Veículo Automóvel Utilitário*. MSc Diss., University of Coimbra, 2011.

[6] Halderman, James D. *Automotive Technology*. 4th ed. New Jersey: Prentice Hall, 2012.

[7] http://enginedesignfunctioncylinder.blogspot.pt/2015_05_01_archive.html
(Accessed 18/06/2016)

[8] http://www.motorteiledirekt.de/media/catalog/product/p/1/p1470371.jpg
(Accessed 30/06/2016)

[9] Silva Alves, Eric. *Optimisation numérique et expérimentale du rendement énergétique du moteur M3165*. Rapport de Stage, Universidade de Coimbra, 2015.

[10] http://www.briskusa.com/sites/default/files/Bbacistheoryofspark.jpg
(Accessed 21/06/2016)

[11] Rototest. *Certificate of Performance*. Sweden: Rototest Research Institute, 2006.

[12] http://www.dacarsa.net/basic/divulgacion/Valvetronic.php
(Accessed 18/06/2016)

[13] Haas, Michael. *UniAir – The first fully-variable, electro-hydraulic valve control system*. Schaeffler Symposium, 2010.

[14]https://upload.wikimedia.org/wikipedia/commons/f/f4/Overhead_valve_with_bucket_tappet_(Autocar_Handbook,_13th_ed,_1935).jpg

(Accessed 02/07/2016)

[15] Antunes, Fernando J. V. *Sebenta de Vibrações e Ruído*. DEM-FCTUC. 2015.

[16] http://www.grumpysperformance.com/vgd5.jpg

(Accessed 02/07/2016)

[17] Budynas, Richard G. and Nisbett, J. Keith. *Shigley's Mechanical Engineering Design*. 9th ed. New York: McGraw-Hill, 2011.

[18] Sandu G., Cofaru C. and Jelerenschi L., *Design of the Cam Profile for a Roller Finger Follower Valve Train*. Transilvania University of Brasov, 2012.

[19]http://toyota-engine.ru/engines/dvigatel-1kr-fe/podrobnoe-opisanie-i-tekhnicheskie-kharakteristiki-dvigatelya-1kr-fe

(Accessed 26/03/2016)

[20] http://world.honda.com/automobile-technology/VTEC/

(Accessed 02/07/2016)

[21] Wan, Mark. *Autozine Techinical School*, http://www.autozine.org/technical_school/engine/vvt_5.html

(Accessed 03/06/2016)

[22] http://www.kfztech.de/kfztechnik/motor/steuerung/valvetronic.htm

(Accessed 02/07/2016)

[23] http://www.not2fast.com/bmw/bmw_valvetronic.jpg

(Accessed 02/07/2016)

[24] http://www.superstreetonline.com/how-to/engine/1405-nissan-variable-valve-timing/

(Accessed 02/07/2016)

[25] http://dbnst.nii.ac.jp/english/detail/1809

(Accessed 02/07/2016)

[26] http://toyota-club.net/files/faq/12-11-03_faq_valvematic_eng.htm

(Accessed 02/07/2016)

[27] http://paultan.org/2007/06/13/toyota-reveals-valvematic-technology/

(Accessed 02/07/2016)

[28] Forno, António. *Alternative organ for controlling the load of four- stroke internal combustion engines and its activation*. MSc Diss., University of Coimbra, 2012.

[29]http://www.germancarforum.com/threads/fiat-multiair-in-detail-incl-bmw-valvetronic-comparison.30583/

(Accessed 02/07/2016)

[30]http://www.carmagazine.co.uk/car-news/industry-news/fiat/tomorrows-world-fiats-multiair-engine-tech/

(Accessed 02/07/2016)

[31]http://www.gizmag.com/fiat-releases-multiair-engine-technology--is-this-a-fundamental-breakthrough-in-internal-combustion-engine-design/11184/pictures

(Accessed 02/07/2016)

[32] Ace Wire Spring & Form Company. *Properties of Common Spring Materials*. United States of America: 1105 Thompson Avenue – Mckees Rocks, PA, 2016.

ANNEX A

- **Other Engine Characteristics**

In an early work phase, the program has to be adjusted to an already existing engine to serve as a starting point. As was referred when defining the engine's characteristics, the Toyota 1KR-FE engine is used as a "model" engine (Figure 0.1 and Table 0.1). This engine is widely used by manufacturers such as Peugeot, Citroen, Daihatsu and Toyota.

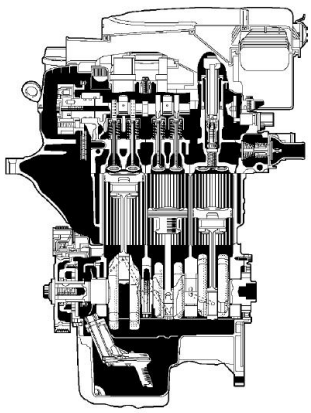

Figure 0.1. 1KR-FE Engine's schematic illustration [19].

Table 0.1. 1KR-FE engine characteristics.

Toyota Optimal Drive 1.0-litre VVT-i petrol	
Engine Code	1KR-FE
Type	Inline 3-cylinder in transverse position
Valve Mechanism	DOHC 12-valve VVT-i
Bore x Stroke [mm]	71.0 x 84.0
Displacement [cm^3]	998
Compression Ratio	10.5:1
Maximum Power [kW] at [rpm]	50.7 at 6000
Maximum Torque [Nm] at [rpm]	93 at 3600

The software's modified parameters are presented below.

1. **Engine's geometric parameters**

- Number of cylinders
- Bore
- Stroke
- Compression ratio
- Connecting rod length

2. **Engine's lubrication parameters**

- Oil type
- Oil crankcase temperature
- Dynamic viscosity of the oil

3. **Intake valves geometric parameters**

- Inlet valve opening
- Inlet valve closing

4. **Exhaust valves geometric parameters**

- Exhaust valve opening
- Exhaust valve closing

5. **Geometric characteristics for the calculation of the engine's friction value**

6. **Piston ring geometric and lubrication characteristics**

- Height and oil film thickness:

i. above the first (compression) piston ring
ii. between the first and second (compression) piston rings
iii. between the second piston ring and the oil scraper ring
iv. of the piston skirt below the oil scraper ring

- Height and oil thickness:

i. of the first piston ring
ii. of the second piston ring
iii. of the oil scraper ring
iv. of the piston skirt below the oil scraper ring

7. **Geometric and lubrication characteristics of connecting rod's and camshaft's bearings**

- Diameter, width and thickness of oil film:

i. of the connecting rod's main bearings

ii. of the connecting rod's head bearings

iii. of the camshaft's main bearings

- Number of:

i. connecting rod's main bearings

ii. connecting rod's head bearings

iii. camshafts

- Medium diameter, width, oil film thickness and width:

i. camshaft's rebounds

8. **Camshaft and connecting rod shaft seal dimensions**

- Inner connecting rod shaft seal diameter on the flywheel side
- Inner connecting rod shaft seal diameter on the supply side
- Inner camshaft shaft seal diameter on the supply side

9. **Water pump specifications**

- Entrance Angle
- Exit Angle
- Transmission Ratio

10. **Oil pump specifications**

ANNEX B

- **Bucket Tappet Valve Train CAD Design**

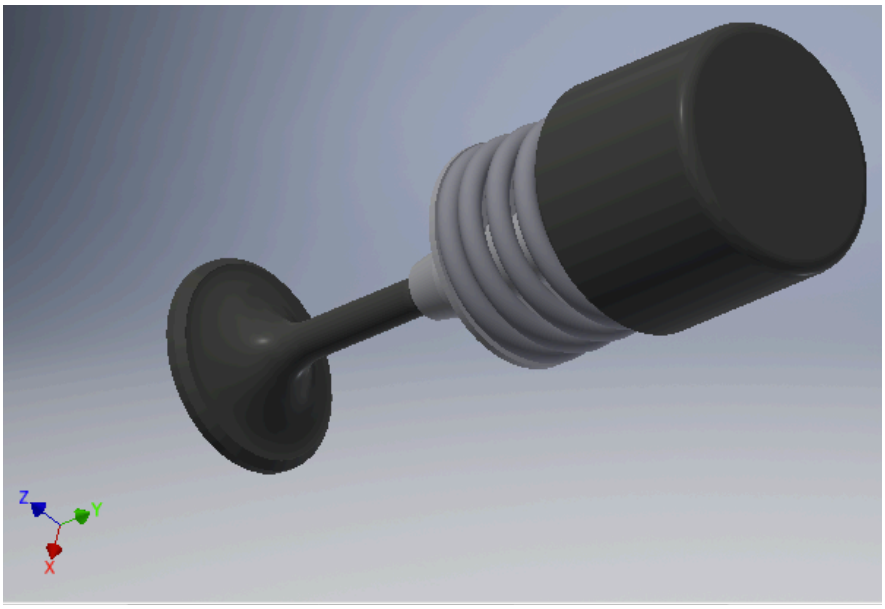

Figure 0.1. Bucket tappet valve train designed in Autodesk Inventor 2016.

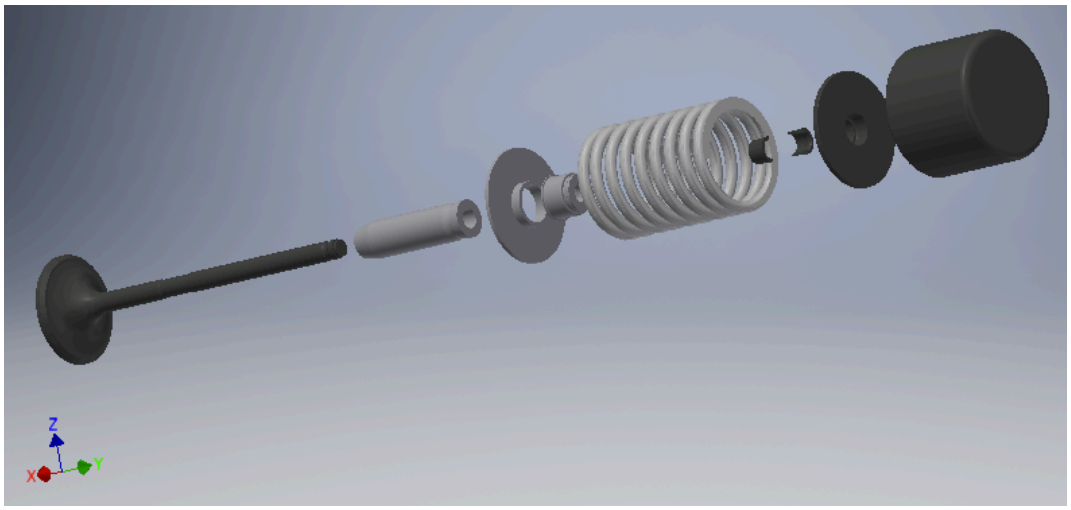

Figure 0.2. Bucket tappet valve train – exploded view - designed in Autodesk Inventor 2016.

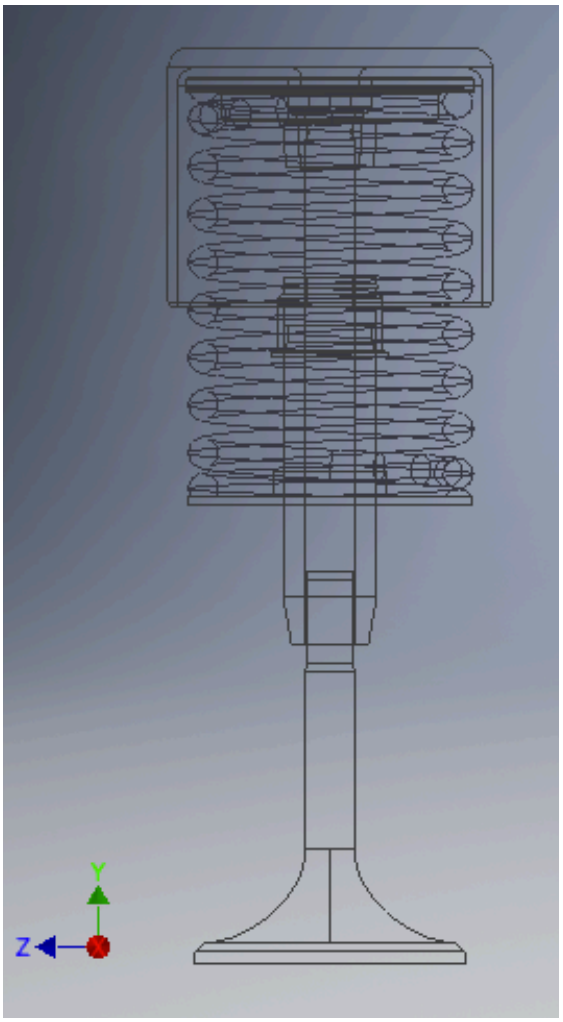

Figure 0.3. Bucket tappet valve train designed in Autodesk Inventor 2016.

ANNEX C

- **Continuous Variable Valve Lift Mechanism**
  - **Analysis**

Presently, there are innumerous variable valve lift solutions, which makes it impractical to analyze them all. Instead, this analysis is centered on the most popular and/or advantageous solutions. There are two (general) types of variable valve lift systems: **discrete** and **continuous** systems. Both of them are designed to work **dependently** or **independently** from the engine's valve timing. Valve trains with transition between cam profiles (discrete) appeared in the 80's, with the first one being the innovative Honda VTEC system. Shortly after, many other car manufacturers did their own interpretation of the VTEC system.

Honda VTEC - VTEC stands for: Variable Valve Timing and Lift Electronic Control. As its designation indicates, this system does not work independently from the valve timing. Its first generation relies on two different cam profiles, as can be seen in Figure 0.1, with the orange cam having a bigger lobe than the blue cam. The blue cam profile actuates the rocker arms at low engine speed (n), while the orange cam is disengaged at this speed (n). When n increases, the orange cam is engaged and actuates the rocker arms, producing a higher lift. Since this system cannot regulate lift and timing independently, the orange cam also produces a greater intake time.

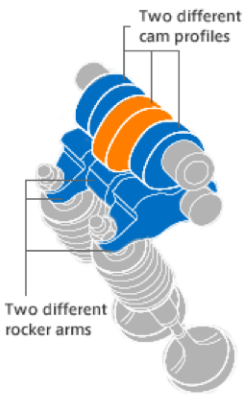

Figure 0.1. Honda's VTEC mechanism [20].

Although this was a breakthrough at the time, there are obvious limitations to what VTEC (and other discrete systems) can do. One of the most important limitations is the

fact that valve lift can't be controlled independently from the valve timing. This is caused by the fact that when a bigger cam lobe comes into effect, not only is the valve lift greater, but also the duration of the intake (a limitation that is also present in some continuous systems). The second limitation is the fact that there isn't a continuous adjustment to the vehicle's needs. Instead, the discrete system works very similarly (in that aspect) to a turbocharger, only coming into effect at a certain n value (which originates the so called "turbocharger lag"). With the arrival of the XXI century came the fully continuous variable valve lift systems. In 2001, BMW released the first system to reach production – the Valvetronic.

BMW Valvetronic - The goal of this system is not to deliver an extra amount of brake power, but instead, to focus on reducing the engine's bsfc alone (BMW reports a 10% reduction in bsfc [19]). Unlike the previously existing discrete valve lift systems, BMW's Valvetronic ensures that valve lift is changed continuously, in order to match the position of the throttle pedal – controlled by the driver. It is a combination between BMW's variable valve timing technology – the Double VANOS – and a variable valve lift mechanism. Together they work as a fully controllable valve train. Although this innovation allows for the throttle butterfly valve to be removed, BMW has chosen to keep it. It is only used on cold starts and as a backup mechanism in case Valvetronic fails. In any other case, the butterfly valve is kept fully open (like if it wasn't there) and only Valvetronic is used.

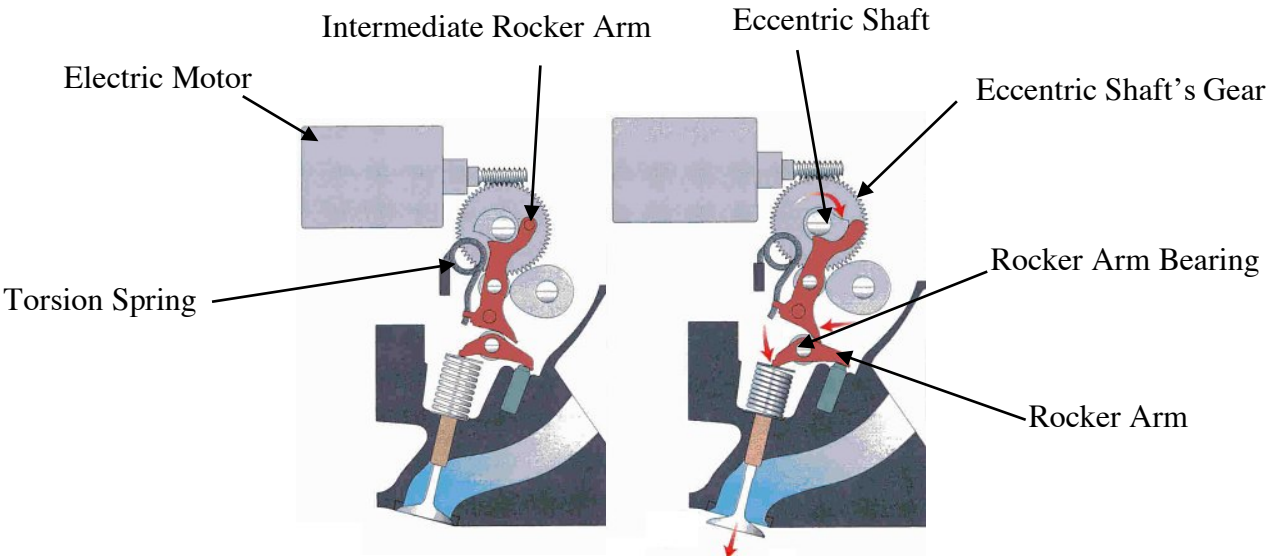

Figure 0.2. BMW's Valvetronic mechanism at minimum (left) and maximum lift (right) positions [21].

The mechanism is presented in Figure 0.2. The electric motor is in contact with the eccentric shaft's gear which allows it to control the angular position of the shaft. The eccentric shaft on the other hand, is in contact with the intermediate rocker arm. The intermediate rocker arm's position will determine a greater or smaller lift of the valve. Once the camshaft pushes the rocker arm's bearing, it will cause the rocker arm to open the valve.

Figure 0.3. BMW's Valvetronic 1st generation [22].

On the left of Figure 0.3 (dyed in green), Valvetronic is on the minimum valve lift position, whereas on the right (dyed in pink), the maximum valve lift position is depicted. On the center of the image it's clear to see the difference in valve lift. One of the biggest advantages of system's such as BMW's Valvetronic is allowing the valve train to operate within any position within the minimum and maximum limits. Although operating according to the same principles, BMW has recently updated and produced a second generation of its Valvetronic system (Figure 0.4), capable of lowering bsfc by 12%.

Figure 0.4. BMW's Valvetronic 2nd generation [23].

Even though it was the first system to allow a new range of valve train possibilities, Valvetronic has some important disadvantages. In first place it only influences a reduction in bsfc, having no positive impact on brake power. Secondly, being a complicated system, the high number of components mean that it has high inertia and friction losses (limiting the maximum possible engine speed (n)). This means that, although there is a reduction in bsfc on part load, there is no increase in brake power on full load (due to this fact, Valvetronic will stop being a solution for BMW's M-Power range new vehicles). Finally, the Valvetronic system also takes up a large space above the cylinder head, which limits its applicability to smaller vehicles.

Table 0.1. Valvetronic's positive and negative aspects.

	Positive Aspects	Negative Aspects
BMW Valvetronic	• Reduces bsfc by 12% (maximum); • Good throttle response (except with high *n*); • Works independently from the variable valve timing system (Double VANOS); • Reduces NO_x and HC emissions;	• Large size; • Complex system; • Only reduces bsfc in part load; • Increases cylinder head height; • High inertia and friction losses; • Not suitable for high *n*; • Does not increase brake power; • Not possible to deactivate valves or cylinders;

Nissan VVEL

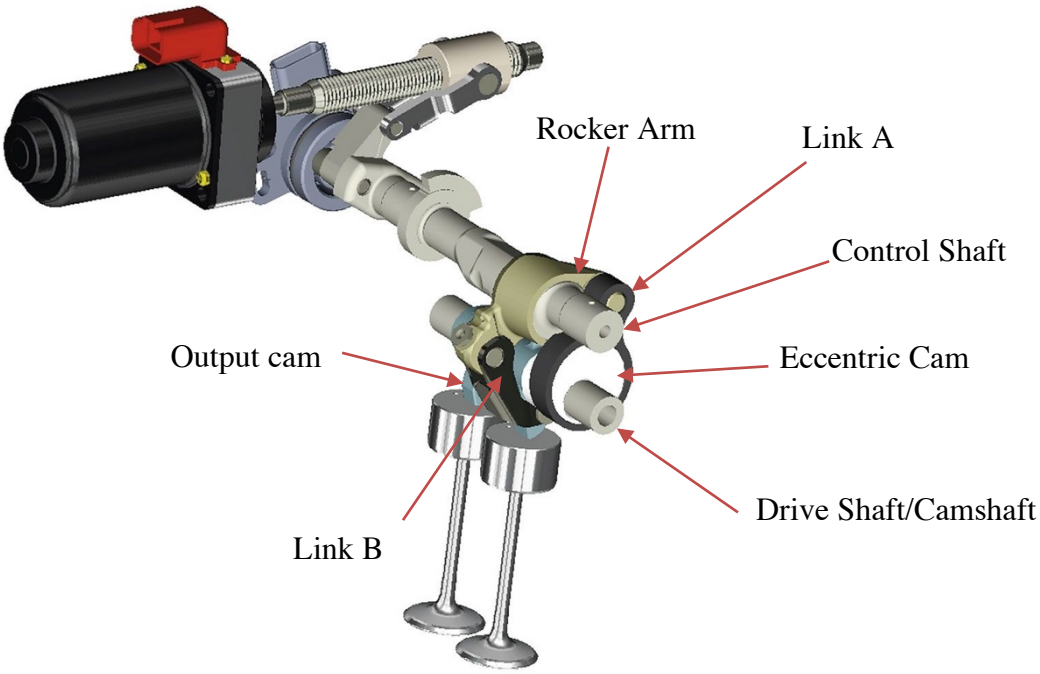

Figure 0.5. Nissan's VVEL mechanism [24].

Six years after BMW's breakthrough, Nissan introduced its VVEL system (Variable Valve Event and Lift). Contrary to the Valvetronic system, this technology cannot work independently from the valve timing. The lift and timing variation are done simultaneously by VVEL, and are mutually dependent. VVEL can achieve a variation in valve lift from 0.7 mm to 12.5 mm. Although still a complicated and bulky system, VVEL benefits from having a shorter design and less components than Valvetronic. This allows it to have a smaller friction energy loss compared to the Valvetronic system, and also to achieve higher n. "The structure consists of two subsystems (Figure 0.5), the mechanical valve train system, to operate the opening and closing of the intake valves, and the actuator system, to vary the valve lift and event angle by controlling the multi-link mechanism of the valve train based on control commands. The VVEL opens and closes the intake valves by transforming the rotating motion of the drive shaft into an oscillating motion of the output cam through the multi-link mechanism (Figure 0.5). The drive shaft, to which input cams (eccentric drive cams) are fixed, corresponds to a conventional camshaft, being synchronized at half crankshaft speed. Above the drive shaft, the system deploys the control shaft integrated with

control cams (eccentric control cams) and the rocker arm actuating (rocking) at the fulcrum at the center of the control cam. The input cam and one end of the rocker arm are connected to each other by link A, which transforms the rotating motion into a rocking motion. The other end of the rocker arm is connected with the output cam by link B, actuating (oscillating) the output cam. As a result, the output cams oscillate at the center of the driveshaft and push down the respective valve lifters. The actuator system consists of a link mechanism, a reduction mechanism, a DC motor and a position sensor (rotating angle sensor). The DC motor rotates the eccentric control cam through the reduction mechanism, varying valve lift and event angle.

Figure 0.6 shows how the system varies the valve lift by changing the attitude of the link mechanism. The fulcrum of the rocker arm has moved its farthest travel towards the driveshaft by shifting the eccentric control cam off-center in the direction of the driveshaft. As a result, the whole attitude of the link mechanism has been changed, allowing the output cam to oscillate with a large angle and hence producing a large valve lift. In counter state of minimum valve lift, the fulcrum of the rocker arm is moved away from the drive shaft and lowering the oscillation angle of the output cam. As a result, the contact length with the valve lift shortens producing a small valve lift." [28].

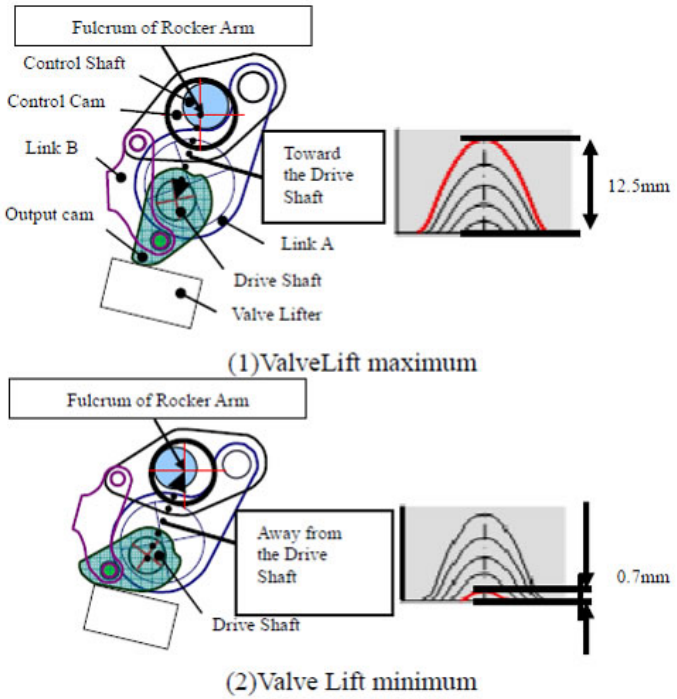

Figure 0.6. Nissan's VVEL mechanism at maximum (up) and minimum lift (down) [25].

The butterfly throttle valve is not completely eliminated but has its role reduced. With this system, Nissan states that there is a reduction in 10% of bsfc at partial load. Another advantage of VVEL is the fact that it can withstand higher *n* than Valvetronic, not compromising top end performance. However, the gain in brake power given by this system (comparing to the same engine without this technology) is largely lost due to the additional friction of the extra components [21].

Table 0.2. VVEL's positive and negative aspects.

Nissan VVEL	• Reduces bsfc by 10% (maximum); • Good throttle response; • Enhanced brake power at high *n*; • Valves or cylinder deactivation possible; • Reduces HC emissions;	• Large size; • Complex system; • Increases cylinder head height (although not as much as Valvetronic); • Expensive; • Doesn't work independently from the variable timing system; • High electrical consumption (electro-mechanical system);

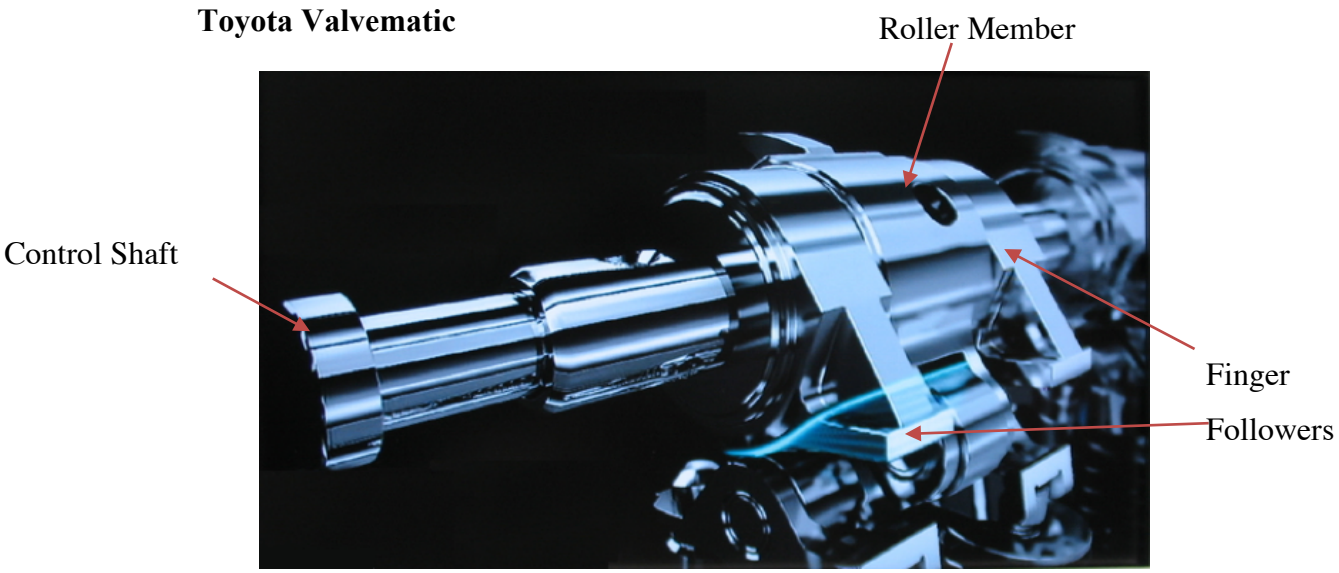

Figure 0.7. Valvematic's intermediate shaft [26].

In 2008 Toyota introduced Valvematic. Having already developed and implemented Dual VVT-i (Variable Valve Timing with Intelligence) technology in their vehicles, Toyota went a step further by adding a mechanism that allows for continuously variable valve lift. Toyota's CVVL solution (Continuous Variable Valve Lift) is notoriously different and simpler from BMW's and even Nissan's complex approach. Valvematic is a compact and simple solution that, unlike the previous two, does not increase the height of the cylinder head. Instead, an intermediate shaft is added to the intake side of the cylinder head (Figure 0.7). The increase in inertia and friction due to the added components is lower (compared to the previously presented technologies), which prevents it from compromising top end power (like Valvetronic). Toyota claims that Valvematic improves brake power by 10% and reduces by 5 to 10% bsfc in regular driving. Valvematic is able to produce a variable lift between 0.97mm and 11mm. This technology saves the need for a throttle butterfly valve, which helps save fuel in part load (it can be maintained for safety reasons).

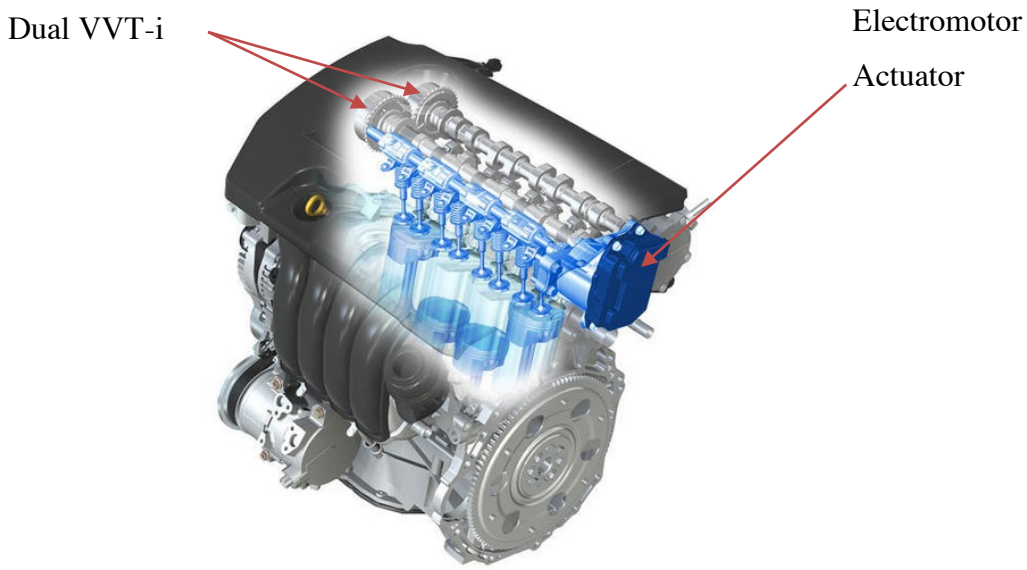

Figure 0.8. Toyota Valvematic [27].

An explanation on how Valvematic operates follows: "Valvematic employs an intermediate shaft (Figure 0.7) to achieve continuous variable valve lift. The intermediate shaft has an actuating member for each cylinder. Each actuating member is made of two finger followers laminating a roller bearing member (Figure 0.7). The finger followers can rotate in relation to the roller member by means of internal gear threads (Figure 0.9) and an electric motor attached to the end of the intermediate shaft (Figure 0.8) Note that the gear threads of roller member and finger followers are in opposite direction (Figure 0.9). This means that when the shaft swivels, the roller member and finger followers will move in opposite direction, moving either apart or closer together. In this way, the axle angle between them can be varied infinitely by the electric motor.

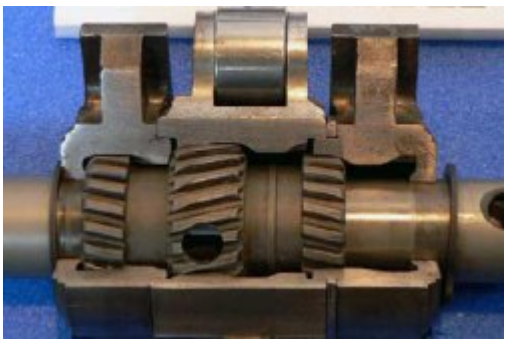

Figure 0.9. Internal gear threads [21].

The intake valve is actuated by the camshaft via intermediate shaft. More precisely speaking, the camshaft acts on the roller member of the intermediate shaft,

transferring the movement to both finger followers, then towards the roller rocker arms and eventually to the intake valves (Figure 0.10). When the finger follower is set at a narrow angle in relation to the roller member, it results in a low valve lift. When the angle of the finger follower is increased, the valve lift is also increased (Figure 0.10). In this way, Valvematic can vary valve lift by adjusting the angle of the finger followers." [21].

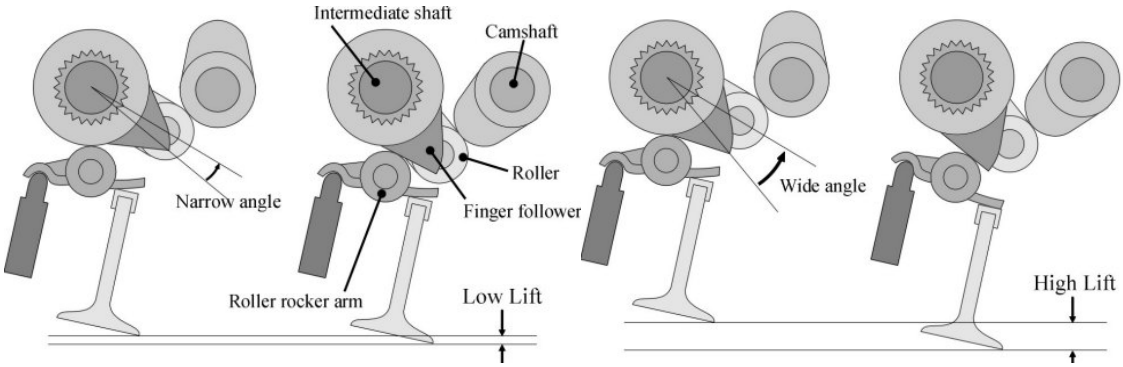

Figure 0.10. Valvematic's low (left) and high (right) lift positions [21].

"The system can be classified into three mechanisms according to their function: the actuator which drives the control shaft which changes valve lift, the variable valve lift mechanism, and the cam phaser which controls intake and exhaust valve timing (Dual VVT-i in Figure 0.8). The actuator (Figure 0.8) consists of a DC brushless motor, a control unit and a mechanism to convert rotary motion into linear motion. It is connected to the control shaft (Figure 0.7), and is positioned in the cylinder head rear end. The DC motor with a rated output torque of about 1 N·m is arranged in a concentric circle around the conversion mechanism for miniaturization of the actuator. When the motor turns the ring gear, the planetary gear revolves around the sun shaft while rotating (Figure 0.11). Because the angle of rotation of the variable arm and cam is always uniform, the range in which the roller rocker arm comes in contact with the oscillation cam changes. The cam surface of the oscillation cam consists of a no lift part and a lift part. This profile affects valve lift height and valve opening duration change. When combined with variable valve timing, this mechanism allows the valve opening and closing event to be controlled independently." [28].

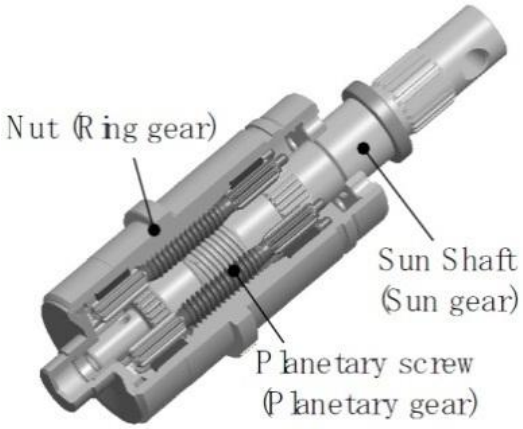

Figure 0.11. Valvematic's mechanism that converts rotary motion into linear motion [28].

Table 0.3. Valvematic's positive and negative aspects.

Toyota Valvematic	• Reduces bsfc (depending on the driving) by 5 to 10% (maximum); • Good throttle response; • Doesn't increase cylinder head height; • Top-end brake power increase of 10 %; • Simple and compact mechanism; • Mechanism is inside the camshaft housing – easier to apply on different engines; • Reduces CO_2 emissions; • Works independently from the variable timing system (Dual VVT-i);	• Not possible to deactivate valves or cylinders; • Power consumption (electro-mechanical system);

FIAT MultiAir

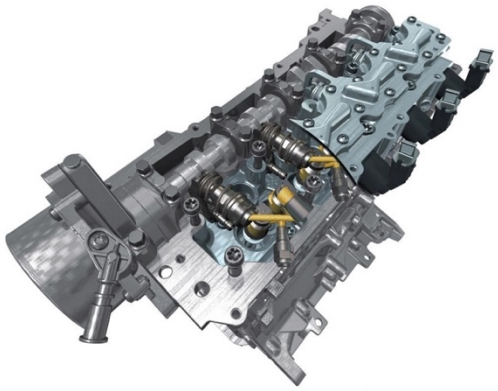

Figure 0.12. FIAT's MultiAir mechanism [29].

MultiAir is an electro-hydraulic system created by FIAT. To understand MultiAir's concept, first it is necessary to consider a DOHC engine – with both intake and exhaust camshafts. MultiAir replaces the intake camshaft of a DOHC engine - as depicted in Figure 0.12. As a result, the formerly designated "exhaust camshaft" is now the engine's only camshaft. Having withdrawn one of the camshafts, the system relies on the remaining one to operate. The camshaft conventionally actuates the exhaust valves while actuating the intake valves through a series of components (Figure 0.13). For this to be possible, an additional cam (per cylinder) is installed on the camshaft (Figure 0.13).

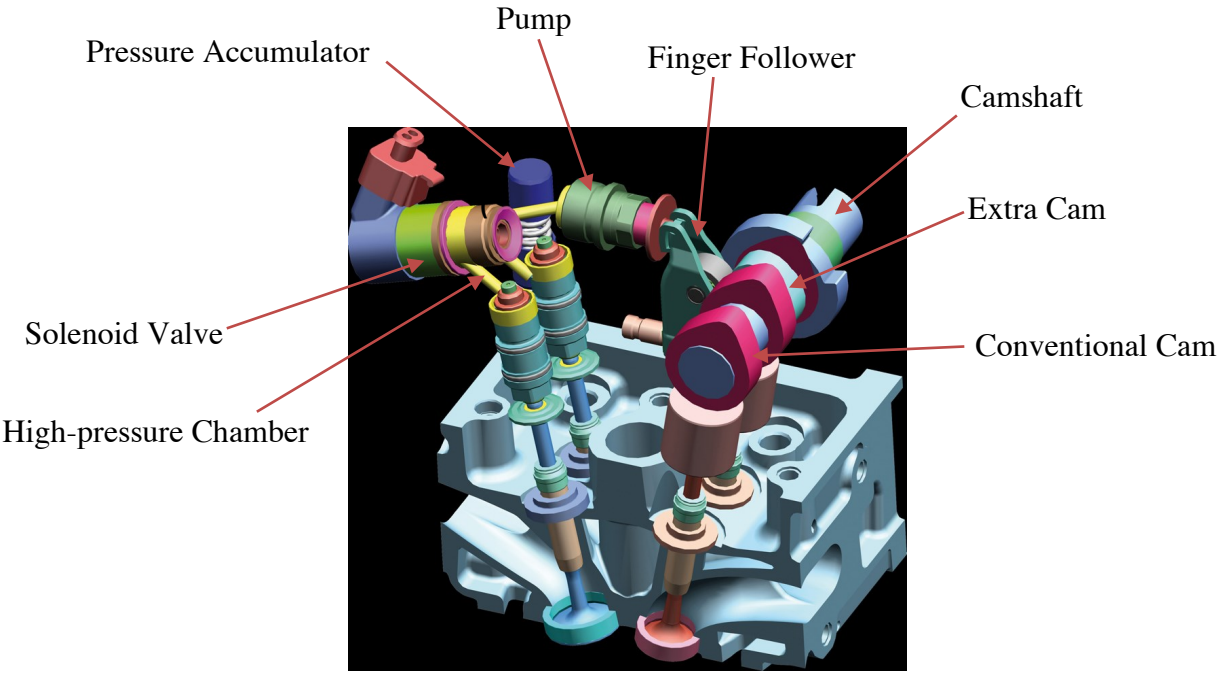

Figure 0.13. A SOHC engine with FIAT's MultiAir technology [30].

"A piston, moved by a mechanical intake cam, is connected to the intake valve through a hydraulic chamber. The valve is controlled by a normally open on/off solenoid valve. When the solenoid valve is closed, the oil in the hydraulic chamber behaves like a solid body and transmits the lift schedule imposed by the mechanical intake cam to the intake valves. When the solenoid valve is open, the hydraulic chamber and the intake valves are de-coupled. The intake valves no longer follow the intake cam and close under the valve spring action. An oil reservoir in the low-pressure part of the oil circuit helps in refilling the high-pressure chamber for the following stroke, thus minimizing energy losses. The final part of the valve closing stroke is controlled by a dedicated hydraulic brake, thus ensuring a soft and regular landing phase in any engine operating condition.

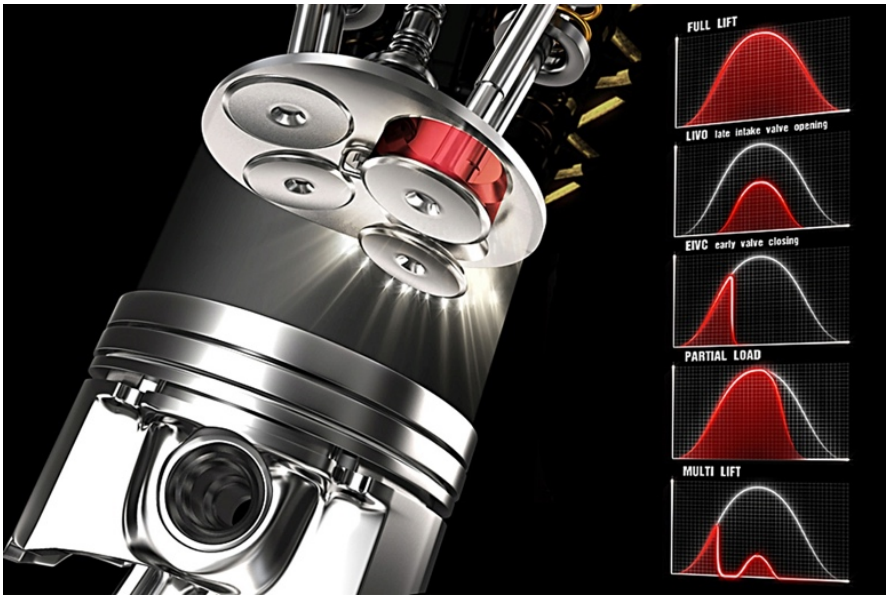

Figure 0.14. MultiAir's actuation modes [31].

Controlling the opening and closing time of the solenoid valve allows a wide range of optimum intake valve opening schedules to be easily obtained (Figure 0.14). For maximum power, the solenoid valve is always closed and full valve opening is achieved. Full opening of the inlet valves is achieved by following the mechanical cam. This maximizes power specifically at high engine speeds (n). In order to increase torque at low revs, the solenoid valve is opened near the end of the cam profile, leading to early intake valve closing. This eliminates the unwanted backflow of fresh air into the manifold and maximizes the air mass trapped in the cylinders. In engine part load conditions, the solenoid valve is opened earlier. The valves are then partially opened to control the trapped air mass

depending on the required torque. Alternatively, the intake valves can be partially opened by closing the solenoid valve once the mechanical cam action has already started. In this case, the air flow into the cylinder is faster and results in higher air turbulence in the combustion chamber. The last two actuation modes can be combined in the same intake stroke, thus generating a so-called "MultiLift" mode that enhances turbulence and the combustion rate at very low loads." [28].

Table 0.4. FIAT MultiAir's positive and negative aspects.

Fiat MultiAir	• Reduces bsfc by 10%; • Good throttle response; • Brake power increase of 10 %; • Ability to change the cam profile; • Flexibility of use: Allows for 5 different actuation modes; • Independent adjustment of each cylinder (with possible deactivation of valves or cylinders) • Low-end torque increased by 15%; • Reduces CO_2 emissions;	• Large size; • Cannot be implemented in both intake and exhaust; • Doesn't include variable valve timing for the exhaust valves;

- **Selection**

Table 0.5. Comparison between the analyzed variable valve lift mechanisms.

	BMW **Valvetronic**	Nissan **VVEL**	Toyota **Valvematic**	FIAT **MultiAir**
Size				
Flexibility				
Easy to Implement				
Reliability				
Fuel Saving				
Power boost				

Having already presented the pros and cons of each system, the overall performance of each mechanism is summarized on Table 0.5. From all four analyzed systems, two obviously stand out: Toyota's Valvematic and FIAT's MultiAir. MultiAir technology is by far the most flexible and innovative thanks to its vast array of possibilities. It truly offers an almost infinite adjustment to the engine's needs. However, it doesn't offer any type of variable valve timing to the exhaust valves, whereas Toyota's Valvematic varies the exhaust valves timing (through its Dual VVT-i technology). Although not as flexible and as innovative as MultiAir, Valvematic is a surprisingly compact and yet powerful solution. It offers more benefits and less limitations than both Valvetronic and VVEL with a much smaller mechanism while still incorporating independent variable valve timing and lift systems.

Throughout the years it is possible to identify some key factors that led to the internal combustion engine's success. Those key factors include the engine's robustness, simplicity and a high power/weight (or even power/size) factor. For all of the previous pointed out reasons, and with these key factors in mind, the chosen mechanism is Toyota's Valvematic.

- **Design**

In this subchapter, the CAD design of Toyota's Valvematic mechanism made in Autodesk Inventor 2016 is presented.

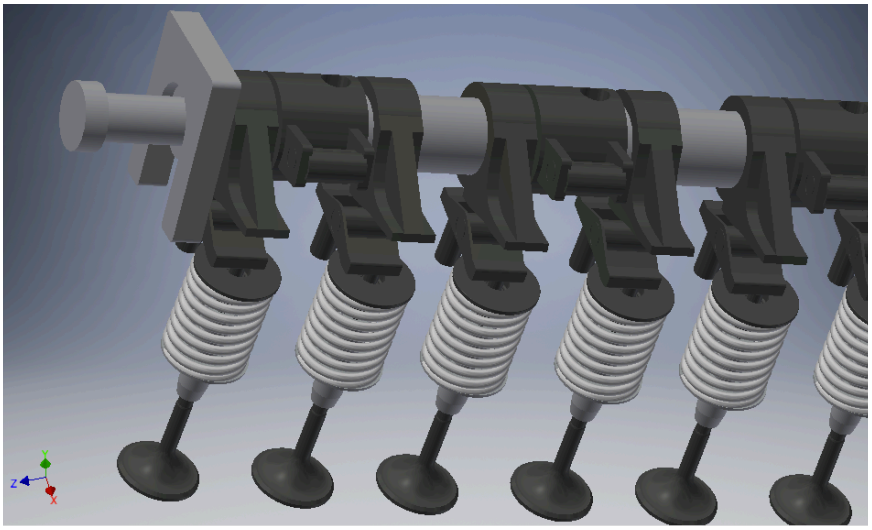

Figure 0.15. Valvematic system designed in Autodesk Inventor 2016.

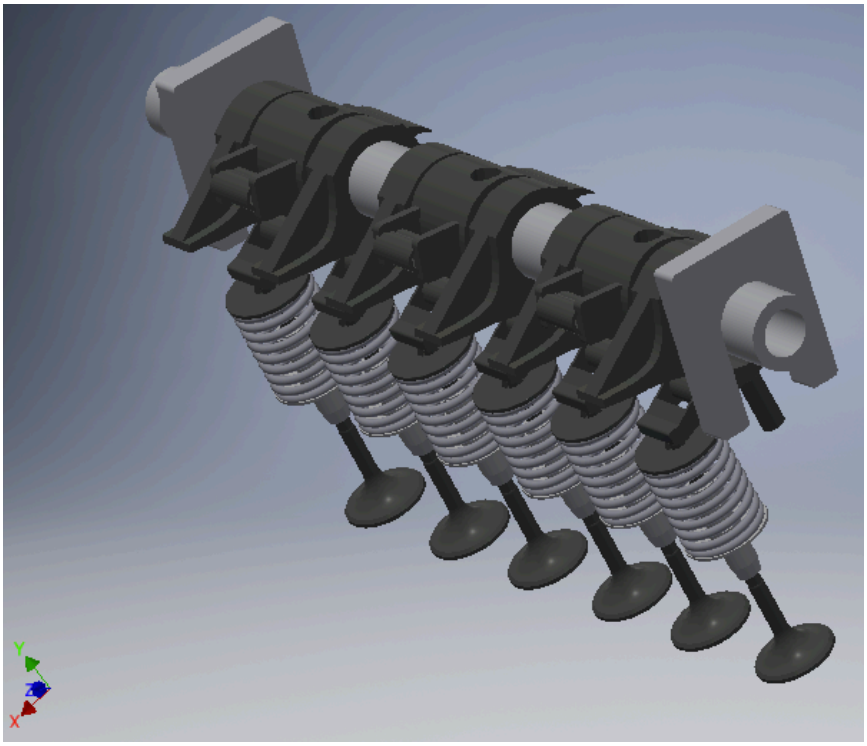

Figure 0.16. Valvematic system designed in Autodesk Inventor 2016.

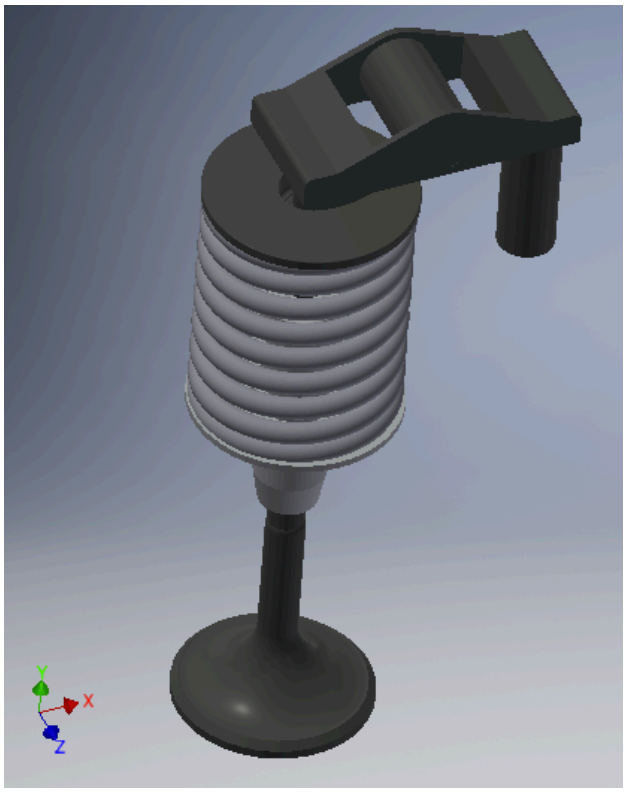

Figure 0.17. Valvematic system designed in Autodesk Inventor 2016.

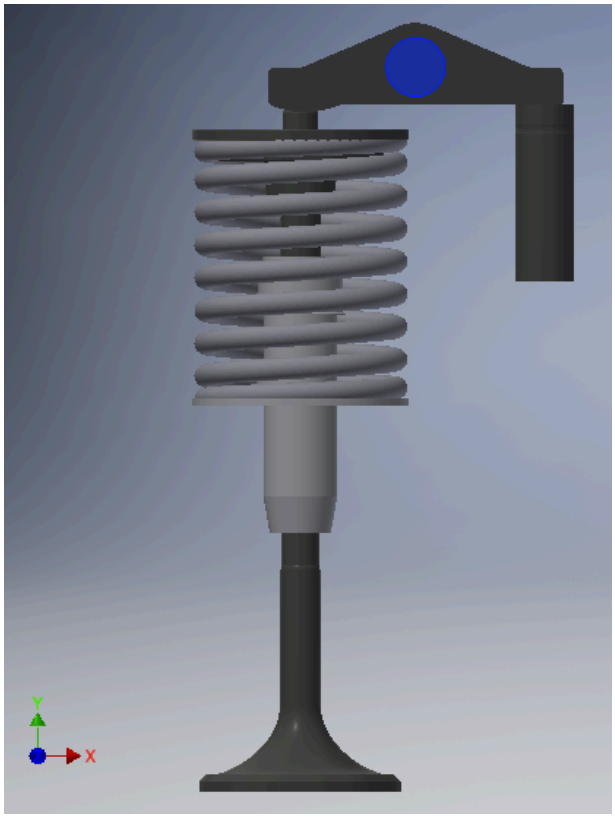

Figure 0.18. Valvematic's finger follower mechanism designed in Autodesk Inventor 2016.